NASA TECHNICAL REPORT

NASA TR R-234

APPLICATION OF LAX'S FINITE-DIFFERENCE METHOD TO NONEQUILIBRIUM HYPERSONIC FLOW PROBLEMS

by Fred R. DeJarnette
Langley Research Center
Langley Station, Hampton, Va.

NATIONAL AERONAUTICS AND SPACE ADMINISTRATION • WASHINGTON, D. C. • MARCH 1966

NASA TR R-234

APPLICATION OF LAX'S FINITE-DIFFERENCE METHOD TO NONEQUILIBRIUM HYPERSONIC FLOW PROBLEMS

By Fred R. DeJarnette

Langley Research Center
Langley Station, Hampton, Va.

NATIONAL AERONAUTICS AND SPACE ADMINISTRATION

For sale by the Clearinghouse for Federal Scientific and Technical Information
Springfield, Virginia 22151 – Price $0.65

APPLICATION OF LAX'S FINITE-DIFFERENCE METHOD TO NONEQUILIBRIUM HYPERSONIC FLOW PROBLEMS

By Fred R. DeJarnette
Langley Research Center

SUMMARY

The finite-difference method developed by P. D. Lax for unsteady flows is applied to the steady-state equations for the supersonic region of inviscid flows past two-dimensional and axisymmetric bodies. A diatomic gas subject to nonequilibrium vibrations and dissociation is considered. As a consequence of Lax's finite-difference scheme, an artificial viscosity is implicitly introduced. This scheme allows the computations to proceed downstream of an initial data line as if no shock wave were present at all. The shock wave appears in the solution, however, smeared over several mesh spaces while it accurately gives the proper jump conditions across the shock.

A new difference scheme is developed for the body points that is more accurate than previously used extrapolation schemes and reflection principles. The numerical results of the present method are shown to compare favorably with the methods of characteristics and integral relations for frozen flow over a cone—parabolic-arc—cylinder, vibrational nonequilibrium flow over a wedge, and chemical nonequilibrium flow of Lighthill's "ideal dissociating gas" over a wedge.

INTRODUCTION

The numerical solution of the inviscid flow field surrounding a vehicle traveling at hypersonic speeds provides a formidable task for computation. At the speeds encountered for a planetary entry, the problem is made more difficult by the presence of nonequilibrium real gas effects. This report develops a finite-difference method for computing the supersonic-hypersonic regions of steady, inviscid flows past two-dimensional and axisymmetric bodies.

Many methods have been formulated and used for nonequilibrium flow-field computations varying from the accurate, but lengthy, method of characteristics (refs. 1 to 3) and inverse blunt-body methods (ref. 4) to the gross, yet simple, method of integral relations (refs. 5 to 7) and stream-tube techniques (ref. 8). In 1954 Lax (ref. 9) introduced a first-order-accuracy difference scheme for computing one-dimensional unsteady flow fields containing shock waves. Roberts (ref. 10) applied this method to spherical waves, and

Bohachevsky et al. (ref. 11) used it to compute steady-state flow fields for two and three dimensions by obtaining the asymptotic solution of the time-dependent flow. More recently, Lax and Wendroff (ref. 12) proposed a finite-difference scheme that is accurate to the second order. Burstein (ref. 13) used this technique to obtain steady flow fields as the asymptotic form of the unsteady flow, whereas Thommen and D'Attorre (ref. 14) applied the difference scheme to the steady-flow equations.

Although the Lax-Wendroff method is accurate to the second order, the numerical computations become prohibitive for a real gas. The numerical method presented here applies the basic difference scheme of the earlier Lax method (ref. 9) to the steady-state flow-field equations. This method represents a good compromise between accuracy and numerical complexities. The governing partial differential equations are first written in conservation (or divergence) form; that is, the coefficients of the derivatives are all unity. The partial derivatives are then replaced with finite-difference quotients, but in such a manner as to introduce implicitly an artificial viscosity. However, the artificial viscosity is due only to the finite-difference scheme employed and differs from that used by VonNeumann and Richtmyer (ref. 15). (VonNeumann and Richtmyer add a viscous pressure term to the static pressure in the differential equations before the difference equations are formed.) As a consequence of the artificial viscosity effect, the computations may proceed downstream of an initial data line as if no shock wave were present at all. The shock wave appears in the solution, however, not as a discontinuity but as a near discontinuity smeared over several mesh spaces while the solution accurately gives the proper jump conditions across the shock wave.

In order to obtain good accuracy on the body surface, a different difference scheme is developed for the body points that is more accurate than the previously used extrapolation schemes (ref. 13) and reflection principles (refs. 11 and 13). The numerical results of the present method are compared with those of the methods of characteristics and integral relations for frozen flow over a cone—parabolic-arc—cylinder, vibrational nonequilibrium flow over a wedge, and chemical nonequilibrium flow of Lighthill's "ideal dissociating gas" over a wedge. The method presented herein is developed in more detail in reference 16.

SYMBOLS

a_m vector defined by equation (16)

b_m vector defined by equation (16)

C^* constant in dissociational rate equation

C_F	locally frozen speed of sound
C_p^*	pressure coefficient, $\frac{2(p - p_\infty)}{\rho_\infty V_\infty^2}$
D	dissociation energy per molecule
d_m	vector defined by equation (16)
E_v	vibrational energy per unit mass
F	function defined by equation (C2)
G	function defined by equation (C3)
H	static enthalpy per unit mass
H_t	total enthalpy per unit mass
j	integer in flow equation; 0 for two-dimensional flow, 1 for axially symmetric flow
K	body curvature
k_B	Boltzmann constant
L	length scale
M	locally frozen Mach number
n,k	number of increments in mesh system (see fig. 2)
N_o	Avogadro's number
p	pressure
r	perpendicular distance from body axis
R	universal gas constant
t	time
T	translational temperature
u	velocity in x-direction
V	magnitude of total velocity

v	velocity in y-direction
W_j	molecular weight of jth species
x	distance along body surface from leading edge (see fig. 1)
y	distance normal to body surface (see fig. 1)
α	atom mass fraction
Γ	rate of dissociation
γ	locally frozen ratio of specific heats
δ	y-position of shock wave
Θ_D	characteristic dissociation temperature, D/k_B
Θ_v	characteristic vibrational temperature
θ	angle between body tangent and axis of symmetry
Λ	vibrational energy rate
λ_x	scale factor in x-direction
μ	locally frozen Mach angle
ξ	Cartesian coordinate along body axis
ρ	mass density
ρ_D	characteristic dissociation density
τ	vibrational relaxation time
ψ	constant defined by equation (10)
$\omega_1,\omega_2,\omega_3,\omega_4,\omega_5$	functions defined by equations (41) and (47)
Ω	shock-wave angle

Subscripts:

A_2	diatomic species
e	equilibrium conditions

F	locally frozen value
n,k	spatial position, $x = x_o + n\,\Delta x$, $y = k\,\Delta y$ (see fig. 2)
o	initial conditions
∞	undisturbed free-stream conditions

Barred quantities are dimensionless as given by equation (7). Unbarred quantities are dimensional.

PROBLEM DEFINITION

General Description

The problem to be studied is the numerical solution of the inviscid, steady supersonic flow over two-dimensional and axisymmetric bodies. The gas model considered is a homonuclear, diatomic gas subject to nonequilibrium vibrations and dissociation. Translation and molecular rotation modes are considered to be completely excited, and electronic excitation and ionization are neglected.

The numerical technique for the flow-field solution is to replace the governing partial differential equations with finite-difference equations. Then, with known flow properties along an initial data line in the supersonic region, the downstream flow field is computed by marching forward in the streamwise direction. Since the numerical technique is restricted to hyperbolic equations, the flow field computed must remain supersonic.

Basic Equations

Figure 1 illustrates the geometry and coordinate system. For this body-oriented coordinate system, x is measured along the surface of the body, y is normal to surface, and the velocity components in these respective directions are u and v. The basic flow equations are written in conservation (or divergence) form as (see ref. 16):

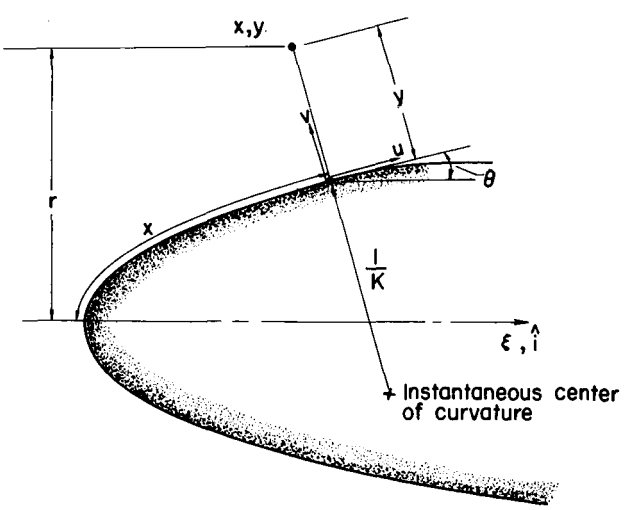

Figure 1.- Body-oriented coordinate system.

Continuity:

$$\frac{\partial\left(\bar{\rho}\bar{u}\bar{r}^{j}\right)}{\partial\bar{x}} + \frac{\partial\left(\bar{\rho}\bar{v}\bar{r}^{j}\lambda_{x}\right)}{\partial\bar{y}} = 0 \tag{1}$$

x-momentum:

$$\frac{\partial\left[\left(\bar{p} + \bar{\rho}\bar{u}^{2}\right)\bar{r}^{j}\right]}{\partial\bar{x}} + \frac{\partial\left(\bar{\rho}\bar{v}\bar{u}\bar{r}^{j}\lambda_{x}\right)}{\partial\bar{y}} + \bar{K}\bar{\rho}\bar{u}\bar{v}\bar{r}^{j} - j\bar{p}\lambda_{x}\sin\theta = 0 \tag{2}$$

y-momentum:

$$\frac{\partial\left(\bar{\rho}\bar{u}\bar{v}\bar{r}^{j}\right)}{\partial\bar{x}} + \frac{\partial\left[\left(\bar{p} + \bar{\rho}\bar{v}^{2}\right)\bar{r}^{j}\lambda_{x}\right]}{\partial\bar{y}} - \bar{K}\left(\bar{p} + \bar{\rho}\bar{u}^{2}\right)\bar{r}^{j} - j\bar{p}\lambda_{x}\cos\theta = 0 \tag{3}$$

Vibrational energy rate:

$$\frac{\partial\left(\bar{\rho}\bar{u}\bar{r}^{j}\bar{E}_{v}\right)}{\partial\bar{x}} + \frac{\partial\left(\bar{\rho}\bar{v}\bar{r}^{j}\lambda_{x}\bar{E}_{v}\right)}{\partial\bar{y}} - \frac{\lambda_{x}\bar{r}^{j}\bar{\rho}LW_{A_2}\Lambda}{V_{\infty}T_{\infty}R} = 0 \tag{4}$$

Rate of dissociation:

$$\frac{\partial\left(\bar{\rho}\bar{u}\bar{r}^{j}\alpha\right)}{\partial\bar{x}} + \frac{\partial\left(\bar{\rho}\bar{v}\bar{r}^{j}\lambda_{x}\alpha\right)}{\partial\bar{y}} - \frac{\lambda_{x}\bar{r}^{j}\bar{\rho}L\Gamma}{V_{\infty}} = 0 \tag{5}$$

Energy:

$$\bar{H} + \frac{\bar{u}^{2} + \bar{v}^{2}}{2} = \bar{H}_{t} = \text{Constant} \tag{6}$$

where $\bar{K} = -\frac{d\theta}{d\bar{x}}$ is the body curvature, $\lambda_x = 1 + \bar{K}\bar{y}$ is the scale factor in the x-direction, and $j = 0$ for two-dimensional body and $j = 1$ for axisymmetric body. The nondimensional vibrational energy is $\bar{E}_v$, α is the atom mass fraction, Λ is the dimensional vibrational rate $\frac{dE_v}{dt}$, and Γ is the dimensional dissociational rate $\frac{d\alpha}{dt}$. All quantities are nondimensionalized as follows (barred quantities are nondimensional):

$$\left.\begin{aligned}
&\bar{u} \text{ or } \bar{v} = \frac{u \text{ or } v}{V_{\infty}} && \bar{H} = \frac{H}{V_{\infty}^{2}} \\
&\bar{T} = \frac{T}{T_{\infty}} && \bar{\Theta}_{D} \text{ or } \bar{\Theta}_{v} = \frac{\Theta_{D} \text{ or } \Theta_{v}}{T_{\infty}} \\
&\bar{E}_{v} = \frac{E_{v}W_{A_2}}{RT_{\infty}} && \bar{\rho} = \frac{\rho}{\rho_{\infty}} \\
&\bar{p} = \frac{p}{\rho_{\infty}V_{\infty}^{2}} && \bar{x},\ \bar{y},\ \text{or } \bar{r} = \frac{x,\ y,\ \text{or } r}{L}
\end{aligned}\right\} \tag{7}$$

The enthalpy and equation of state are, respectively,

$$\bar{H} = \psi\left[\frac{7 + 3\alpha}{2}\bar{T} + (1 - \alpha)\bar{E}_v + \alpha\bar{\Theta}_D\right] \tag{8}$$

$$\bar{p} = \bar{\rho}\bar{T}(1 + \alpha)\psi \tag{9}$$

where

$$\psi \equiv \frac{RT_\infty}{W_{A_2}V_\infty^2} = \left[\gamma_\infty(1 + \alpha_\infty)M_\infty^2\right]^{-1} \tag{10}$$

The locally frozen ratio of specific heats is

$$\gamma = \frac{7 + 3\alpha}{5 + \alpha} \tag{11}$$

and the locally frozen Mach number is

$$M = \left(\frac{u^2 + v^2}{\frac{\gamma p}{\rho}}\right)^{1/2} = \left[\frac{(u^2 + v^2)W_{A_2}}{\gamma(1 + \alpha)RT}\right]^{1/2} \tag{12}$$

Vibrational Nonequilibrium Gas Model

The vibrational nonequilibrium gas model is for a diatomic gas with no dissociation. Therefore, $\alpha = 0$ everywhere and the dissociational rate equation (eq. (5)) is not needed. The vibrational energy rate and relaxation time used here are the same as those used in references 1 and 5; the vibrational energy rate is

$$\Lambda = \frac{E_{v,e} - E_v}{\tau}$$

where the local equilibrium vibrational energy is

$$E_{v,e} = \frac{R\Theta_v}{W_{A_2}\left(e^{\Theta_v/T} - 1\right)}$$

and the vibrational relaxation time τ is given by

$$\tau p \propto \exp\left(\frac{1.3965 \times 10^6}{T}\right)^{1/3}$$

where the temperature is in ^{o}K.

Lighthill Gas Model

A convenient simplification is achieved when the gas model is reduced to Lighthill's ideal dissociating gas of reference 17. This gas model is used in this report for comparative purposes only. The essential features of the gas model are:

(1) The vibrational energy always has one-half of its fully excited classical value; that is,

$$E_v = \frac{RT}{2W_{A_2}}$$

(2) The characteristic density of dissociation ρ_D is considered to be constant.

As a consequence of these simplifications, equation (4) is not required, the enthalpy given by equation (8) is reduced (for Lighthill gas) to

$$\overline{H} = \psi\left[(4 + \alpha)\overline{T} + \alpha\overline{\Theta}_D\right] \tag{13}$$

and the locally frozen ratio of specific heats given by equation (11) is changed (for Lighthill gas) to

$$\gamma = \frac{4 + \alpha}{3} \tag{14}$$

With the exception of equations (4), (8), and (11), the flow-field equations given by equations (1) to (12) also hold for the Lighthill gas.

The dissociational rate equation

$$\Gamma = C^*\rho T^{-2.5}\left[(1 - \alpha)e^{-\Theta_D/T} - \frac{\rho}{\rho_D}\alpha^2\right]$$

which was used in references 3 and 7 (where C^* is a constant) is also used herein.

Boundary Conditions

Since the velocity at the boundary must be tangent to the body surface, $v = 0$ at $y = 0$. The numerical technique developed here does not consider the shock wave as a boundary or a discontinuity. Therefore, there are no boundary conditions to be satisfied at the shock wave since the initial data line extends into the free stream.

METHOD FOR NUMERICAL COMPUTATIONS

Let the flow field be divided into an orthogonal mesh system as shown in figure 2. If the mesh spacings Δx and Δy remain constant, the coordinates of the mesh point n,k are $x = x_0 + n\,\Delta x$ and $y = k\,\Delta y$. Note, however, that the arc length from n,k to

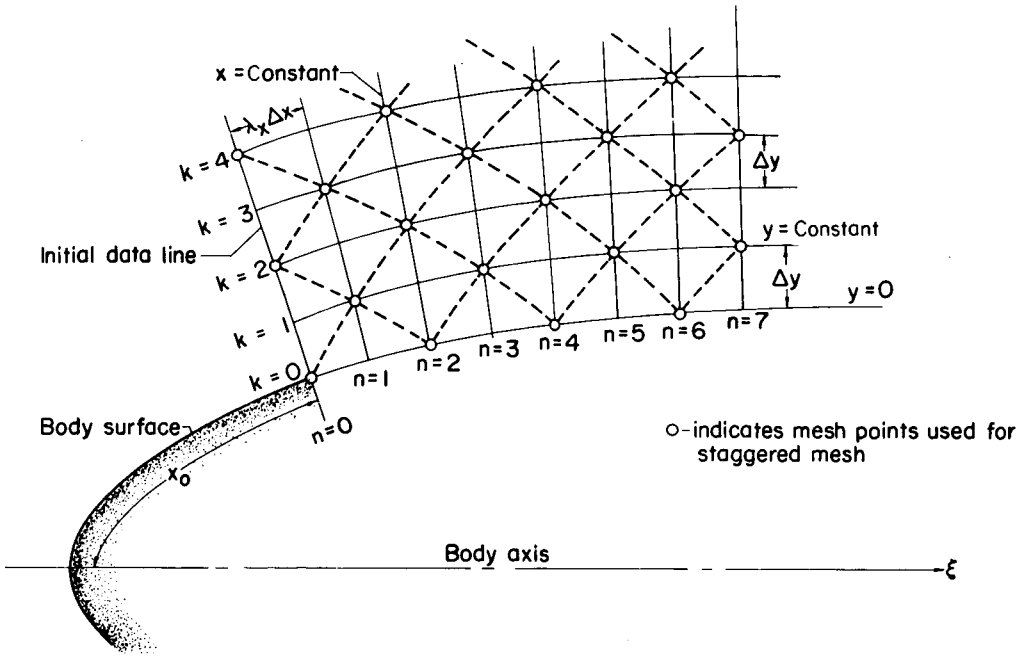

Figure 2.- Mesh system.

n+1,k is $\lambda_x \Delta x$, whereas the linear length from n,k to n,k+1 is Δy. (See fig. 3.) In some applications Δx may vary with n. For these cases

$$x = x_o + \sum_{i=1}^{n} (\Delta x)_i$$

The numerical technique for the flow-field solution is to replace the differential equations with finite-difference equations. Then, with known initial data along the mesh points at n = 0 (obtained from some other technique), new data are computed along the mesh points at n = 1. This technique is continued for increasing values of n. In this manner the flow-field properties are computed at the various mesh points throughout the supersonic portion of the flow field. Since the differential equations are hyperbolic, the ratio $\Delta x/\Delta y$ is bounded. If this bound is exceeded, the numerical computations become unstable. The proper stability criterion is discussed subsequently.

The system of partial differential equations, given by equations (1) to (5), may be written as one vector equation:

$$\frac{\partial a_m}{\partial \bar{x}} + \frac{\partial b_m}{\partial \bar{y}} + d_m = 0 \qquad (m = 1, 2, 3, 4, 5) \qquad (15)$$

where

$$\left.\begin{array}{lll} a_1 = \bar{\rho}\bar{u}\bar{r}^j & b_1 = \bar{\rho}\bar{v}\bar{r}^j\lambda_x & d_1 = 0 \\ a_2 = (\bar{p} + \bar{\rho}\bar{u}2)\bar{r}^j & b_2 = b_1\bar{u} & d_2 = \overline{K}a_3 - j\bar{p}\lambda_x \sin\theta \\ a_3 = a_1\bar{v} & b_3 = (\bar{p} + \bar{\rho}\bar{v}2)\bar{r}^j\lambda_x & d_3 = -\overline{K}a_2 - j\bar{p}\lambda_x \cos\theta \\ a_4 = a_1\overline{E}_v & b_4 = b_1\overline{E}_v & d_4 = \dfrac{-\lambda_x\bar{r}^j\Lambda\bar{\rho}LWA_2}{V_\infty T_\infty R} \\ a_5 = a_1\alpha & b_5 = b_1\alpha & d_5 = \dfrac{-\lambda_x\bar{r}^j L\bar{\rho}\Gamma}{V_\infty} \end{array}\right\} \qquad (16)$$

The difference scheme, suggested by Lax (ref. 9), replaces the partial derivative $\left(\frac{\partial a_m}{\partial \bar{x}}\right)_{n,k}$ at the mesh point n,k with the modified forward difference quotient

$$\frac{(a_m)_{n+1,k} - \frac{1}{2}\left[(a_m)_{n,k+1} + (a_m)_{n,k-1}\right]}{\Delta\bar{x}}$$

and replaces $\left(\frac{\partial b_m}{\partial \bar{y}}\right)_{n,k}$ with the symmetric difference quotient

$$\frac{(b_m)_{n,k+1} - (b_m)_{n,k-1}}{2\,\Delta\bar{y}}$$

Since only the mesh points $n,k+1$ and $n,k-1$ are involved at n for both of these difference quotients, the term $(d_m)_{n,k}$ is replaced by the average value

$$\frac{1}{2}\left[(d_m)_{n,k+1} - (d_m)_{n,k-1}\right]$$

With these substitutions the system of partial differential equations

$$\left(\frac{\partial a_m}{\partial \bar{x}}\right)_{n,k} + \left(\frac{\partial b_m}{\partial \bar{y}}\right)_{n,k} + (d_m)_{n,k} = 0 \qquad (m = 1, 2, 3, 4, 5)$$

are replaced with

$$(a_m)_{n+1,k} = \frac{1}{2}\left[(a_m)_{n,k+1} + (a_m)_{n,k-1}\right] - \frac{\Delta\bar{x}}{2\,\Delta\bar{y}}\left[(b_m)_{n,k+1} - (b_m)_{n,k-1}\right]$$

$$- \frac{\Delta\bar{x}}{2}\left[(d_m)_{n,k+1} + (d_m)_{n,k-1}\right] \qquad (17)$$

for $m = 1, 2, 3, 4, 5$. In this manner $(a_m)_{n+1,k}$ may be evaluated in terms of a_m, b_m, and d_m at the mesh points $n,k+1$ and $n,k-1$. Therefore, if the quantities a_m

are known at $n = 0$ and $k = 0, 2, 4, \ldots$, the values of a_m can be determined at all points of the staggered mesh $n = 1, 2, 3, \ldots$ and $k = 1, 3, 5, 7, \ldots$ when n is odd; and $k = 0, 2, 4, 6$ when n is even. (See fig. 2.)

If equation (17) is used for $k = 0$, then imaginary flow properties are required at the mesh point $n,-1$ which is inside the body. Since the computational procedure cannot determine these properties at $k = -1$, a different finite-difference scheme is developed later for the body points.

The significance of the finite-difference scheme employed here is more readily seen when equation (17) is rearranged as

$$\frac{(a_m)_{n+1,k} - (a_m)_{n,k}}{\Delta\bar{x}} + \frac{(b_m)_{n,k+1} - (b_m)_{n,k-1}}{2\,\Delta\bar{y}} + (d_m)_{n,k}$$

$$= \frac{(\Delta y)^2}{2\,\Delta\bar{x}}\left[\frac{(a_m - \Delta\bar{x}d_m)_{n,k+1} - 2(a_m - \Delta\bar{x}d_m)_{n,k} + (a_m - \Delta\bar{x}d_m)_{n,k-1}}{(\Delta\bar{y})^2}\right] \tag{18}$$

The conventional manner of forming finite differences is to replace $\left(\frac{\partial a_m}{\partial\bar{x}}\right)_{n,k}$ with the forward difference quotient

$$\frac{(a_m)_{n+1,k} - (a_m)_{n,k}}{\Delta\bar{x}}$$

to replace $\left(\frac{\partial b_m}{\partial\bar{y}}\right)_{n,k}$ with the symmetric difference quotient

$$\frac{(b_m)_{n,k+1} - (b_m)_{n,k-1}}{2\,\Delta\bar{y}}$$

and to replace the second derivative $\left[\frac{\partial^2(a_m - \Delta\bar{x}d_m)}{\partial\bar{y}^2}\right]_{n,k}$ with

$$\frac{(a_m - \Delta\bar{x}d_m)_{n,k+1} - 2(a_m - \Delta\bar{x}d_m)_{n,k} + (a_m - \Delta\bar{x}d_m)_{n,k-1}}{(\Delta\bar{y})^2}$$

Therefore, the differential equation that corresponds to the difference equation (17) using conventional difference quotients is

$$\frac{\partial a_m}{\partial\bar{x}} + \frac{\partial b_m}{\partial\bar{y}} + d_m = \frac{(\Delta\bar{y})^2}{2(\Delta\bar{x})}\,\frac{\partial^2(a_m - \Delta\bar{x}d_m)}{\partial\bar{y}^2} \tag{19}$$

This differential equation differs from that shown as equation (15) by the addition of the second derivative term on the right-hand side. In comparison with the momentum equation for a viscous fluid (see ref. 18), the additional term in equation (19) is similar to part

of the viscous terms in the viscous momentum equation. However, the "artificial" coefficient of viscosity $\frac{(\Delta\bar{y})^2}{2\,\Delta\bar{x}}$ is not a function of the fluid properties, as it is in the viscous momentum equation, but is a function of the mesh spacing only. Also, as the mesh spacing approaches zero, this coefficient approaches zero. The effect of the additional term involving the second derivative is designated in references 9 and 10 as an "artificial viscosity." It tends to smooth out discontinuous and rapidly varying flow variables when they arise.

One such discontinuity that appears in the inviscid solution of supersonic flow over bodies is a shock wave. Normally, the shock wave is taken as a boundary, and the Rankine-Hugoniot equations specify the boundary conditions. However, a numerical solution of the viscous Navier-Stokes equations yields a shock-wave structure in which the fluid properties are not discontinuous, but vary continuously over a narrow distance. (See ref. 19.) The introduction of "artificial" viscosity in equation (18) gives this same qualitative effect, but the shock-wave thickness predicted is too large because the viscosity effect is not real. A simple example of the numerical computation of the flow of a perfect gas through an oblique shock wave illustrates this point and is given in appendix A.

An important feature of the present method is that shock waves are not regarded as discontinuities and the numerical solution proceeds as if no such waves were present at all. However, the shock waves appear in the final solution not as a discontinuity but as a near-discontinuity smeared over several mesh spaces. As a result, there are no boundary conditions to be satisfied at the shock wave itself; for some fluid problems this simplification is a significant one. Although the shock-wave thickness in the solutions is incorrect, the flow fields on both sides are accurately described. (See the example in appendix A.) The success of the difference scheme presented here is due, in part, to the divergence form of the differential equations and, in part, to the artificial viscosity effect. The difference scheme of equation (17) is accurate to $0(\Delta\bar{x}^2)$. (See ref. 16 for the details.)

Stability Criterion

Consider the two adjacent mesh points $n,k+1$ and $n,k-1$ in a flow field. As has been shown, the flow properties at these two points are used to determine those at the point $n+1,k$. Since the numerical technique used here is restricted to supersonic flow, the mesh point $n+1,k$ must lie within the Mach triangle about the points $n,k+1$ and $n,k-1$. (See fig. 3.) This criterion is the classical Courant-Friedrichs-Lewy stability criterion (ref. 20) used by Lax (ref. 9) and Roberts (ref. 10).

The Mach triangle is the triangle formed by the line joining $n,k-1$ and $n,k+1$, the left-running Mach line from $n,k-1$, and the right-running Mach line from $n,k+1$. As pointed out by Wood and Kirkwood (ref. 21), the appropriate Mach line for a reacting gas

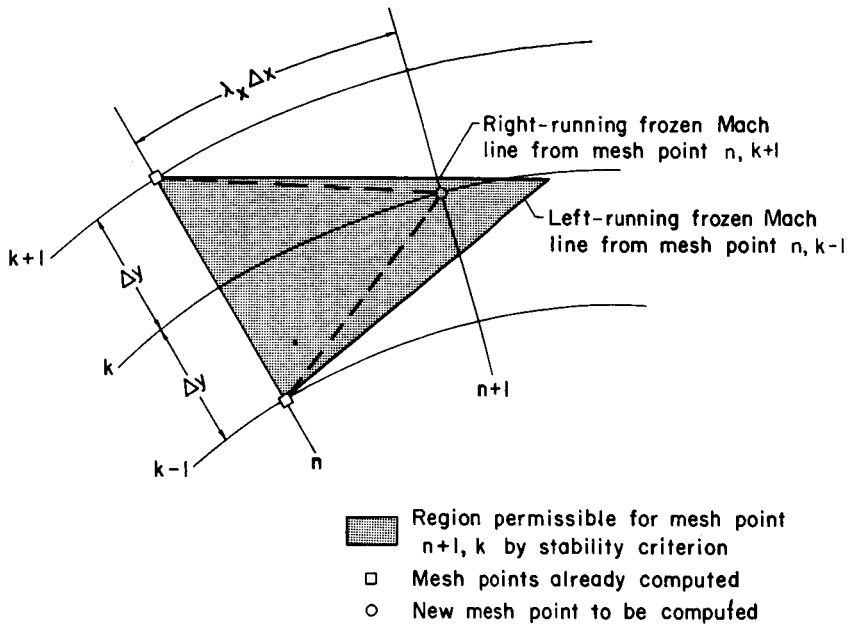

Figure 3.- Stability criterion.

is that determined by the locally frozen Mach number; that is,

$$\sin \mu = \frac{1}{M} \qquad (M \geq 1) \qquad (20)$$

where μ is the angle between the locally frozen Mach line and the streamline. Therefore, in the $\bar{x},\bar{y}$ coordinate system used here, the slopes of the frozen Mach lines are given by

$$\frac{1}{\lambda_x}\left(\frac{d\bar{y}}{d\bar{x}}\right)_{\pm} = \tan\left[\tan^{-1}\left(\frac{\bar{v}}{\bar{u}}\right) \pm \mu\right]$$

After considerable rearrangement, this equation becomes

$$\frac{1}{\lambda_x}\left(\frac{d\bar{y}}{d\bar{x}}\right)_{\pm} = \frac{\dfrac{\bar{u}\bar{v}}{\bar{C}_F{}^2} \pm \left(\dfrac{\bar{u}^2 + \bar{v}^2}{\bar{C}_F{}^2} - 1\right)^{1/2}}{\dfrac{\bar{u}^2}{\bar{C}_F{}^2} - 1} \qquad (21)$$

where

$$\bar{C}_F{}^2 = \frac{\gamma \bar{p}}{\bar{\rho}}$$

When $\frac{\bar{u}}{\bar{C}_F} = 1$, $\left(\frac{d\bar{y}}{d\bar{x}}\right)_{\pm} = \pm\infty$ for $\bar{v} = 0$, $\left(\frac{d\bar{y}}{d\bar{x}}\right)_{+} = +\infty$ and $\left(\frac{d\bar{y}}{d\bar{x}}\right)_{-}$ is finite for $\bar{v} > 0$, and $\left(\frac{d\bar{y}}{d\bar{x}}\right)_{-} = -\infty$ and $\left(\frac{d\bar{y}}{d\bar{x}}\right)_{+}$ is finite for $v < 0$. Therefore, at least one of the Mach lines is parallel to the $\bar{y}$-axis when $\frac{\bar{u}}{\bar{C}_F} = 1$. This same result may also be deduced from the fact that the velocity component normal to a frozen Mach line has the magnitude of the frozen speed of sound.

Equation (21) may be used to write the stability criterion as

$$\frac{\Delta\bar{x}}{\Delta\bar{y}} \leqq \left\{ \frac{\left[\left(\frac{\bar{u}}{\bar{C}_F}\right)^2 - 1\right]\left(\frac{1}{\lambda_x}\right)}{\frac{\bar{u}|\bar{v}|}{\bar{C}_F^2} + \left(\frac{\bar{u}^2 + \bar{v}^2}{\bar{C}_F^2} - 1\right)^{1/2}} \right\}_{\min} \tag{22}$$

Therefore, in order to have $\Delta\bar{x}/\Delta\bar{y}$ finite and positive, it is necessary to have

$$\frac{\bar{u}}{\bar{C}_F} > 1$$

Note that since $\frac{\bar{u}}{\bar{C}_F} \leqq M$, $\frac{\bar{u}}{\bar{C}_F} > 1$ is a more stringent requirement than $M > 1$.

Individual Fluid Properties

For mesh points away from the body, $k \geqq 1$, equation (17) gives $(a_m)_{n+1,k}$ in terms of the known properties at $n,k+1$ and $n,k-1$. A method is given below whereby the individual fluid properties can be obtained from a_m. Since

$$a_1 = \bar{\rho}\bar{u}\bar{r}^j$$

$$a_2 = (\bar{p} + \bar{\rho}\bar{u}^2)\bar{r}^j$$

$$a_3 = a_1\bar{v}$$

$$a_4 = a_1\bar{E}_v$$

$$a_5 = a_1\alpha$$

it is immediately evident that

$$\bar{v} = \frac{a_3}{a_1} \tag{23}$$

$$\bar{E}_v = \frac{a_4}{a_1} \tag{24}$$

$$\alpha = \frac{a_5}{a_1} \tag{25}$$

The other properties are more involved. The ratio $\frac{a_2}{a_1}$ gives

$$\frac{a_2}{a_1} = \frac{\bar{p}}{\bar{\rho}\bar{u}} + \bar{u} \tag{26}$$

or

$$\bar{u}^2 - \frac{a_2}{a_1}\bar{u} + \frac{\bar{p}}{\bar{\rho}} = 0 \tag{27}$$

The $\frac{\bar{p}}{\bar{\rho}}$ term in this equation can be obtained as a function of $\bar{u}$, $\bar{v}$, $\bar{E}_v$, and α from the energy equation and the equation of state as

$$\frac{\bar{p}}{\bar{\rho}} = \frac{\bar{H}_t - (1 - \alpha)\bar{E}_v\psi - \alpha\bar{\Theta}_D\psi - \frac{\bar{v}^2}{2}}{\frac{7 + 3\alpha}{2(1 + \alpha)}} - \frac{\bar{u}^2}{\frac{7 + 3\alpha}{1 + \alpha}} \tag{28}$$

Substitute equation (28) into equation (27) to get

$$\frac{6 + 2\alpha}{7 + 3\alpha}\bar{u}^2 - \frac{a_2}{a_1}\bar{u} + \frac{\bar{H}_t - (1 - \alpha)\bar{E}_v\psi - \alpha\bar{\Theta}_D\psi - \frac{\bar{v}^2}{2}}{\frac{7 + 3\alpha}{2(1 + \alpha)}} = 0 \tag{29}$$

and, the solution of this quadratic equation is

$$\bar{u} = \frac{\frac{a_2}{a_1} \pm \left\{\left(\frac{a_2}{a_1}\right)^2 - \frac{8(1 + \alpha)(6 + 2\alpha)}{(7 + 3\alpha)^2}\left[\bar{H}_t - (1 - \alpha)\bar{E}_v\psi - \alpha\bar{\Theta}_D\psi - \frac{\bar{v}^2}{2}\right]\right\}^{1/2}}{\frac{2(6 + 2\alpha)}{7 + 3\alpha}} \tag{30}$$

From a physical standpoint $\bar{u}$ must be real and single valued at every position in the flow field. Thus, the term under the radical must be positive or zero, and the sign preceding this term must be appropriately chosen. To investigate these requirements, the restrictions necessary to make equation (30) an identity will be determined.

From equation (26),

$$\frac{a_2}{a_1} = \frac{\bar{p}}{\bar{\rho}\bar{u}} + \bar{u} = \bar{u}\left(\frac{\bar{p}}{\bar{\rho}\bar{u}^2} + 1\right)$$

and equation (28) yields

$$\frac{8(1+\alpha)(6+2\alpha)}{(7+3\alpha)^2}\left[\bar{H}_t - (1-\alpha)\bar{E}_v\psi - \alpha\bar{\Theta}_D\psi - \frac{\bar{v}^2}{2}\right] = \frac{8(3+\alpha)}{7+3\alpha}\bar{u}^2\left(\frac{\bar{p}}{\bar{\rho}\bar{u}^2} + \frac{1+\alpha}{7+3\alpha}\right)$$

Hence, the term under the radical in equation (30) becomes

$$\left(\frac{a_2}{a_1}\right)^2 - \frac{8(1+\alpha)(6+2\alpha)}{(7+3\alpha)^2}\left[\bar{H}_t - (1-\alpha)\bar{E}_v\psi - \alpha\bar{\Theta}_D\psi - \frac{\bar{v}^2}{2}\right] = \left[\frac{\bar{u}(5+\alpha)}{7+3\alpha}\right]^2\left[1 - \frac{(7+3\alpha)\bar{p}}{(5+\alpha)\bar{\rho}\bar{u}^2}\right]^2$$

This relation shows that the term under the square root sign is always nonnegative. Since the nondimensional frozen speed of sound is

$$\bar{C}_F = \frac{C_F}{V_\infty} = \left(\frac{\gamma\bar{p}}{\bar{\rho}}\right)^{1/2} = \left(\frac{7+3\alpha}{5+\alpha}\frac{\bar{p}}{\bar{\rho}}\right)^{1/2}$$

equation (30) becomes

$$\bar{u} = \frac{\bar{u}\left[\left(\frac{5+\alpha}{7+3\alpha}\right)\frac{\bar{C}_F^2}{\bar{u}^2} + 1\right] \pm \left\{\left[\frac{\bar{u}(5+\alpha)}{7+3\alpha}\right]^2\left(1 - \frac{\bar{C}_F^2}{\bar{u}^2}\right)^2\right\}^{1/2}}{\frac{4(3+\alpha)}{7+3\alpha}}$$

If it is noted that

$$\bar{u} > 0$$

$$0 \leq \alpha \leq 1$$

and

$$\left[\left(1 - \frac{\bar{C}_F^2}{\bar{u}^2}\right)^2\right]^{1/2} = \left|1 - \frac{\bar{C}_F^2}{\bar{u}^2}\right|$$

equation (30) becomes an identity if the positive sign is chosen when

$$1 - \frac{\bar{C}_F^2}{\bar{u}^2} \geq 0$$

and the negative sign is selected for

$$1 - \frac{\bar{C}_F^2}{\bar{u}^2} \leq 0$$

The stability criterion for supersonic flow (eq. (22)) requires that $1 - \frac{\bar{C}_F^2}{\bar{u}^2} > 0$. Therefore, the positive sign must be used in equation (30) and, as a result,

$$\bar{u} = \frac{\frac{a_2}{a_1} + \left\{\left(\frac{a_2}{a_1}\right)^2 - \frac{8(1+\alpha)(6+2\alpha)}{(7+3\alpha)^2}\left[\bar{H}_t - (1-\alpha)\bar{E}_v\psi - \alpha\bar{\Theta}_D\psi - \frac{\bar{v}^2}{2}\right]\right\}^{1/2}}{\frac{2(6+2\alpha)}{7+3\alpha}} \tag{31}$$

The remaining flow properties may now be computed from equations (16) and (9) as

$$\bar{\rho} = \frac{a_1}{\bar{u}\bar{r}^j} \tag{32}$$

$$\bar{p} = \frac{a_2 - a_1\bar{u}}{\bar{r}^j} \tag{33}$$

and

$$\bar{T} = \frac{\bar{p}}{\bar{\rho}(1+\alpha)\psi} \tag{34}$$

For Lighthill's gas a_4 is not required; hence,

$$\bar{v} = \frac{a_3}{a_1} \tag{35}$$

and

$$\alpha = \frac{a_5}{a_1}$$

and in a manner similar to that given previously

$$\bar{u} = \frac{\frac{a_2}{a_1} + \left[\left(\frac{a_2}{a_1}\right)^2 - \frac{2(7+\alpha)(1+\alpha)}{(4+\alpha)^2}\left(\bar{H}_t - \alpha\bar{\Theta}_D\psi - \frac{\bar{v}^2}{2}\right)\right]^{1/2}}{\frac{7+\alpha}{4+\alpha}} \tag{36}$$

(for Lighthill gas). Then $\bar{\rho}$, $\bar{p}$, and $\bar{T}$ may be determined from equations (32), (33), and (34).

Body Points

As previously mentioned, the finite-difference scheme of equation (17) can be used for the body point $n+1,0$ only if imaginary flow properties are known at the point $n,-1$ inside the body. Since the computational procedure cannot determine the properties at

k = -1, these properties must be determined by an extrapolation scheme or reflection principle. Several extrapolation and reflection techniques (such as those in ref. 13) were tested in the computation of the frozen flow past a wedge (for which the exact solution is known) by the present method. However, the results showed that the properties computed at the body points by all these techniques were less accurate than those computed by the method given herein.

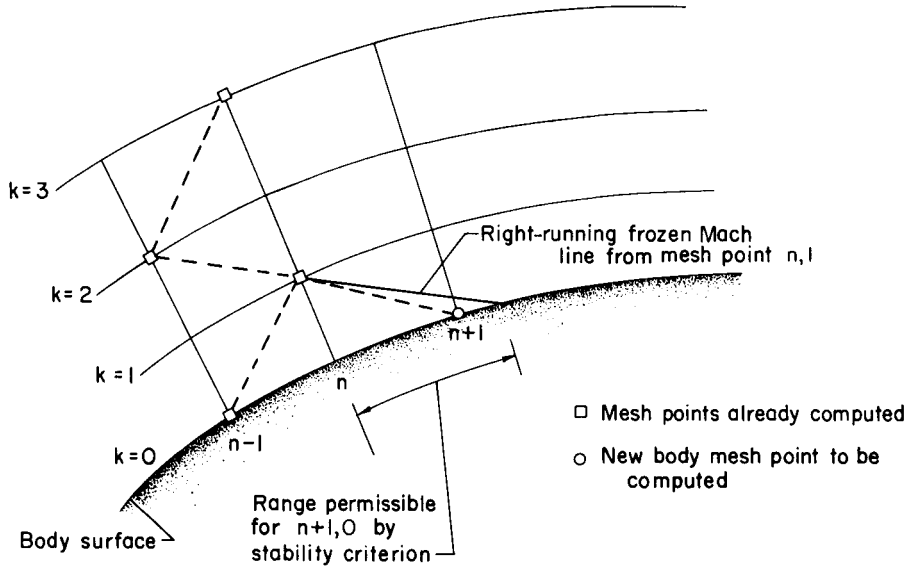

Figure 4.- Mesh system at body surface.

It was found that more accurate results were obtained when the properties at mesh points n-1,0 and n,1 were used to determine the properties at the body point n+1,0 as illustrated in figure 4. The finite-difference scheme replaces $\left(\frac{\partial a_m}{\partial \bar{x}}\right)_{n,0}$ by the symmetrical difference quotient

$$\frac{(a_m)_{n+1,0} - (a_m)_{n-1,0}}{2\,\Delta\bar{x}}$$

replaces $\left(\frac{\partial b_m}{\partial \bar{y}}\right)_{n,0}$ by the modified forward difference quotient

$$\frac{(b_m)_{n,1} - \frac{1}{2}\left[(b_m)_{n+1,0} + (b_m)_{n-1,0}\right]}{\Delta\bar{y}}$$

and replaces $(d_m)_{n,0}$ by the average value

$$\frac{1}{2}\left[(d_m)_{n+1,0} + (d_m)_{n-1,0}\right]$$

With these replacements, the system of partial differential equations

$$\left(\frac{\partial a_m}{\partial \bar{x}} + \frac{\partial b_m}{\partial \bar{y}} + d_m\right)_{n,0} = 0 \qquad (m = 1, 2, 3, 4, 5)$$

become

$$(a_m + \Delta\bar{x}d_m)_{n+1,0} = (a_m - \Delta\bar{x}d_m)_{n-1,0} - \frac{2\,\Delta\bar{x}}{\Delta\bar{y}}\left\{(b_m)_{n,1} - \frac{1}{2}\left[(b_m)_{n+1,0} + (b_m)_{n-1,0}\right]\right\} \tag{37}$$

for $m = 1, 2, 3, 4, 5$.

At first glance equation (37) appears to be insufficient because $(d_m)_{n+1,0}$ and $(b_m)_{n+1,0}$ appear, and the properties at $n+1,0$ are unknown. However, because of the coordinate system used, there are two simplifications which allow a solution to be obtained. First, the $m = 3$ vector is not required because $a_3 = \bar{\rho}\bar{u}\bar{v}\bar{r}^j$ and the boundary condition on the body requires that $v_{n+1,0} = 0$ for all values of n; hence, $(a_3)_{n+1,0} = 0$. Second, since

$$b_1 = \bar{\rho}\bar{v}\bar{r}^j\lambda_x$$

$$b_2 = b_1\bar{u}$$

$$b_4 = b_1\overline{E}_v$$

$$b_5 = b_1\alpha$$

$(b_m)_{n+1,0} = (b_m)_{n-1,0} = 0$ for $m = 1, 2, 4, 5$. With these simplifications, equation (37) becomes

$$(a_m + \Delta\bar{x}d_m)_{n+1,0} = (a_m - \Delta\bar{x}d_m)_{n-1,0} - \frac{2\,\Delta\bar{x}}{\Delta\bar{y}}(b_m)_{n,1} \tag{38}$$

for $m = 1, 2, 4, 5$.

For mesh points on the body, equation (38) gives $(a_m + \Delta\bar{x}d_m)_{n+1,0}$ in terms of the known properties at $n,1$ and $n-1,0$ for $m = 1, 2, 4, 5$. Also, it has previously been shown that $(a_3)_{n+1,0} = 0$ and $(d_1)_{n+1,0} = 0$. Explicit relations for the individual fluid properties can be obtained for a perfect (frozen) gas only, since d_4 and d_5 are zero for these gases.

At the body surface, $\bar{v} = 0$, $\bar{y} = 0$, $\lambda_x = 1$, and $d_2 = -jp \sin \theta$; therefore,

$$\frac{a_2 + \Delta\bar{x}d_2}{a_1} = \frac{\bar{p}}{\bar{\rho}\bar{u}}\left(1 - \frac{j\,\Delta\bar{x} \sin \theta}{\bar{r}}\right) + \bar{u} \tag{39}$$

Substitute equation (28) for $\frac{\bar{p}}{\bar{\rho}}$ into this equation to obtain

$$\omega_1\bar{u}^2 + \omega_2\bar{u} + \omega_3 = 0 \tag{40}$$

where

$$\left.\begin{aligned} \omega_1 &= 1 - \frac{1 + \alpha}{7 + 3\alpha}\left(1 - \frac{j\,\Delta\bar{x} \sin \theta}{\bar{r}}\right) \\ \omega_2 &= -\frac{a_2 + \Delta\bar{x}d_2}{a_1} \\ \omega_3 &= \left[\bar{H}_t - (1 - \alpha)\bar{E}_v\psi - \alpha\bar{\Theta}_D\psi\right]\frac{2(1 + \alpha)}{7 + 3\alpha}\left(1 - \frac{j\,\Delta\bar{x} \sin \theta}{\bar{r}}\right) \end{aligned}\right\} \tag{41}$$

The solution of equation (40) for supersonic flow is

$$\bar{u} = \frac{-\omega_2 + \left(\omega_2^2 - 4\omega_1\omega_3\right)^{1/2}}{2\omega_1} \tag{42}$$

Equation (42) gives an explicit relation for $\bar{u}$ on the surface for a perfect (frozen) gas since

$$\alpha = \text{Constant}$$

and

$$\bar{E}_v = \text{Constant}$$

for a frozen gas. The other surface variables may be determined now from

$$\bar{\rho} = \frac{a_1}{\bar{u}\bar{r}^j} \tag{43}$$

$$\bar{p} = \frac{\left(a_2 + \Delta\bar{x}d_2\right) - \bar{u}\left(a_1\right)}{\bar{r}^j - j\,\Delta\bar{x} \sin \theta} \tag{44}$$

and

$$\bar{T} = \frac{\bar{p}}{\bar{\rho}(1 + \alpha)\psi} \tag{45}$$

For the nonequilibrium gas, α and $\bar{E}_v$ are not known and the quantities $(a_m + \Delta\bar{x}d_m)_{n+1,0}$ for $m = 1, 2, 4,$ and 5 cannot determine them explicitly. Therefore, an iterative technique must be used; one such technique is described in appendix B.

To illustrate the accuracy of the present method compared with the reflection principle, the frozen flow over a 40.02° wedge was computed for $\gamma = 1.4$ and $M_\infty = 6$. The reflection principle sets

$$u_{n,-1} = u_{n,1}$$

$$\rho_{n,-1} = \rho_{n,1}$$

$$p_{n,-1} = p_{n,1}$$

$$v_{n,-1} = -v_{n,1}$$

and uses equation (17) on the body surface. Figure 5 shows the density along the surface of the wedge. The superiority of the present method over the reflection principle is clearly evident here. Actually, the reflection principle should be more accurate for a straight body than a curved body because it gives incorrect gradients normal to the surface of a curved body. (For instance, the reflection principle yields $\frac{\partial p}{\partial y} = 0$ on the surface, but the centrifugal effects make $\frac{\partial p}{\partial y} \neq 0$ on a curved surface.)

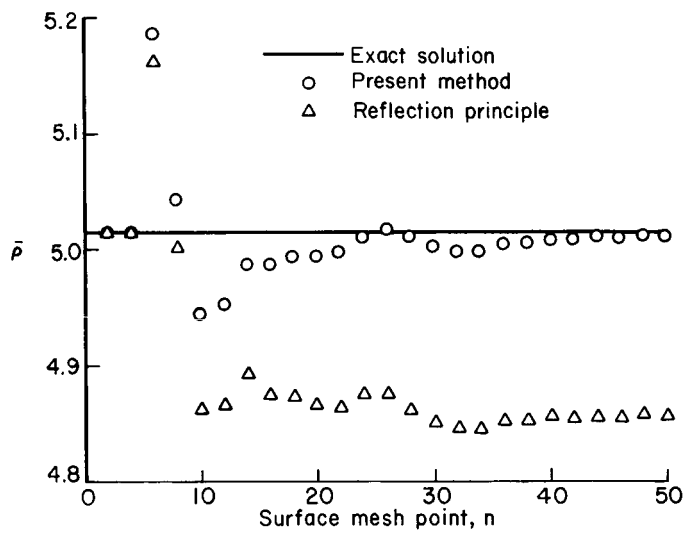

Figure 5.- Density along wedge surface for frozen flow. $M_\infty = 6$; $\gamma = 1.4$; $\theta = 40.02^\circ$.

For the Lighthill gas, the equation analogous to equation (42) is

$$\bar{u} = \frac{\dfrac{a_2 + \Delta\bar{x}d_2}{a_1} + \left[\left(\dfrac{a_2 + \Delta\bar{x}d_2}{a_1}\right)^2 - 4\omega_4\omega_5\right]^{1/2}}{2\omega_4} \tag{46}$$

where

$$\left.\begin{aligned} \omega_4 &= 1 - \frac{1+\alpha}{2(4+\alpha)}\left(1 - \frac{j\,\Delta\bar{x}\sin\theta}{\bar{r}}\right) \\ \text{and} \\ \omega_5 &= \frac{\left(\bar{H}_t - \alpha\bar{\Theta}_D\psi\right)(1+\alpha)}{4+\alpha}\left(1 - \frac{j\,\Delta\bar{x}\sin\theta}{\bar{r}}\right) \end{aligned}\right\} \tag{47}$$

The quantities $\bar{\rho}$, $\bar{p}$, and $\bar{T}$ may then be obtained from equations (43), (44), and (45), respectively.

As shown in reference 22, the proper stability criterion for the body points, in supersonic flow, is that the $n+1,0$ mesh point should not fall beyond the intersection of the right-running frozen Mach line, from $n,1$, with the body surface. (See fig. 4.) Equation (38) is consistent with equation (17) in that it is accurate to $0(\Delta\bar{x}^2)$.

RESULTS

The numerical technique developed herein is applied to frozen flow over a cone—parabolic-arc—cylinder, vibrational nonequilibrium flow over a wedge, and flow of Lighthill's gas over a wedge. These results are compared with the methods of characteristics and integral relations. Additional results for coupled nonequilibrium vibration and dissociation are given in reference 16. All the numerical computations were made on an electronic data processing system.

As has been mentioned, the present method is applicable only to flow regions where the local frozen Mach number is greater than unity. For the case of a pointed body, with an attached bow shock wave, the entire flow field is generally supersonic. The flow in the vicinity of the nose may be approximated by using the frozen flow properties or by using the tip gradients derived for two-dimensional bodies in references 3, 5, and 23. This approximation gives the (initial) flow properties required for the present method to compute the entire flow field.

When the flow over a blunted body is considered, the subsonic-transonic region in the vicinity of the nose must first be determined by some other method, such as that of reference 4 or 6. Such results can then be used to establish the initial data line for the present method, the solution continuing downstream in the supersonic flow region over the body.

Frozen Flow Over a Cone—Parabolic-Arc—Cylinder

This example illustrates the accuracy of the present method for supersonic flow ($M_\infty = 2$, $\gamma = 1.4$) over an axially symmetric body with a discontinuous curvature, but having a continuous slope. Figure 6 shows the body shape. The cone—parabolic-arc junction lies at $\bar{\xi} = 0.05$, and the parabolic-arc—cylinder junction lies at $\bar{\xi} = 0.5$. Note that the tip of the cone is not at $\bar{\xi} = 0$, but at $\bar{\xi} = -0.002777$.

The initial data line was chosen to be the line normal to the surface at the cone—parabolic-arc junction. Since the flow is still conical along this line, the Taylor-Maccoll cone solution (ref. 24) could be used for the flow properties. Three mesh points were chosen inside the shock layer: $k = 0$ on the surface, $k = 2$ midway between the surface and the shock wave, and $k = 4$ just aft of the shock wave. The other points on the initial data line ($k = 6, 8, 10, \ldots$) were in the undisturbed free stream. With $\Delta\bar{y} = 0.0045946$, $\Delta\bar{x} = 0.00459$ for $\bar{\xi} \leq 0.5$, and $\Delta\bar{x} = 0.0055$ for $\bar{\xi} > 0.5$, the flow field was computed as far as $\bar{\xi} = 1.05$. Since $\Delta\bar{y}$ remains constant and the distance between the body and the shock wave increases with $\bar{\xi}$, the number of mesh points inside the shock layer becomes much greater than three as the computations proceed downstream. The time required by the computing machine for this flow field was 2.2 minutes.

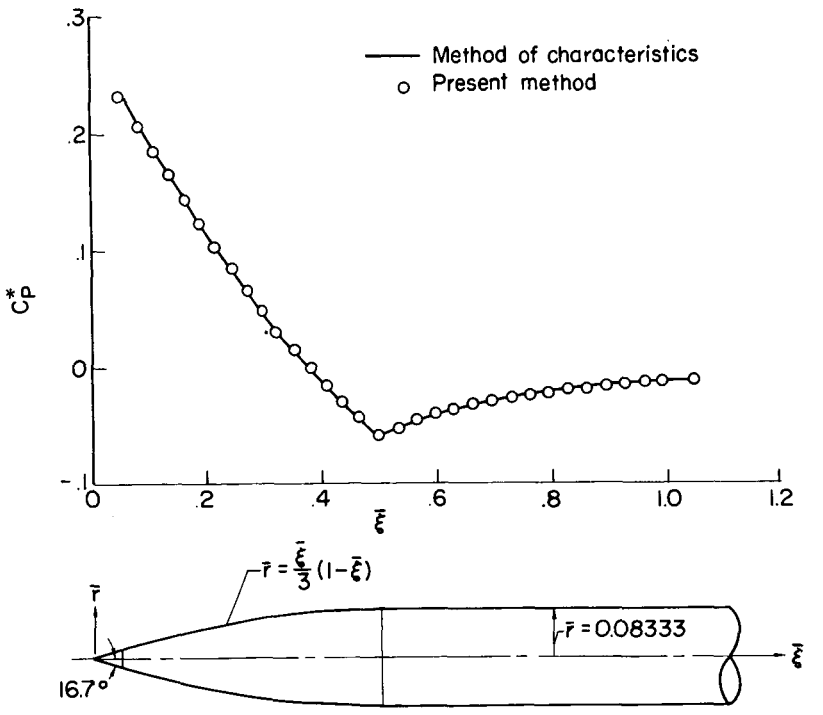

Figure 6.- Variation of surface pressure coefficient with axial distance for frozen flow past a cone—parabolic-arc—cylinder. $M_\infty = 2$; $\gamma = 1.4$; $C_p^* = \frac{2(p - p_\infty)}{\rho_\infty V_\infty^2}$.

The pressure coefficient along the body surface is plotted in figure 6 along with that given by the (standard) method of characteristics. This figure shows good agreement between the two methods.

Nonequilibrium Flow Over Wedges

It is well-known that for the supersonic, inviscid flow of a frozen gas past a wedge, the attached shock wave is straight and the fluid properties are constant between the body surface and the wave. The same qualitative results also hold for a gas in equilibrium; however, in this case, the shock wave is closer to the body and the constant fluid properties are different from those of frozen flow. In particular, the equilibrium pressure and temperature are less than the corresponding properties for frozen flow.

When the conditions are such that nonequilibrium effects must be considered, the flow field is complicated. At the tip of the wedge the flow is frozen since it has just passed through the infinitesimally thin shock wave and has not had time to relax. The translational and rotational energy modes reach equilibrium almost immediately; however, the vibrational and dissociational energies require a finite time to reach equilibrium. For an undissociated free stream, the vibrational energy and the degree of dissociation increase along the surface of the wedge. These conditions in turn decrease the temperature and pressure, but increase the velocity and density. The shock wave is inclined at the angle for frozen flow at the tip, but bends downward and approaches the equilibrium angle far downstream. As the flow along the surface achieves an equilibrium condition downstream, the pressure is the same as that for the equilibrium wedge solution; however, the same is not true for the other flow variables (ref. 1). Downstream of the nose, three regions are observed in the profiles of properties between the body and the shock wave. Near the surface there exists an entropy layer since the streamlines passed through the steeper shock wave near the tip of the wedge. In the vicinity of the shock wave, the flow properties are close to being frozen since they have just passed through the shock wave and have not had time to relax. Between these two regions is a region which is essentially in equilibrium. This portion of the flow field has passed through the shock wave further upstream and thus has had time to relax to the equilibrium conditions.

The wedge was chosen, both for simplicity and for comparison with other methods, in order to investigate the use of the present method for nonequilibrium flows. For the initial data line, a line normal to the surface and at a finite distance from the tip has been used for each case. The flow properties along this line have been determined (approximately) by using the exact wedge-tip gradients given in appendix C.

It was found that an initial data line with only two points between the wedge and the shock wave produced good results. In each case these two points were chosen as $k = 0$ at $y/\delta = 0$, and $k = 2$ at $y/\delta = 2/3$. The remainder of the initial data line ($k = 4, 6, 8, \ldots$) values were free-stream quantities. The distance of the initial data line from the tip $\bar{x}_0$ determines the spacing $\Delta\bar{y}$, whereas $\Delta\bar{x}$ is limited by the stability criterion. Care must be exercised to insure that $\Delta\bar{x}$ remains small compared with the relaxation lengths.

Since the computations extend through the shock wave, the free stream, as well as the shock layer, must be considered in determining the stability criterion. In all the examples considered, the free-stream stability criterion was more stringent than that of the shock layer. This difference is due to the fact that the free-stream velocity is inclined at the wedge half-angle θ to the coordinate system.

As noted by Lax (ref. 9) and demonstrated in appendix A, the shock waves are narrowest when $\Delta\bar{x}$ is chosen as large as possible but still satisfies the stability criterion. Therefore, in the examples given, the largest value of $\Delta\bar{x}$ consistent with the stability criterion was used. It was found that this value was always small compared with the relaxation lengths of vibration and dissociation.

Vibrational nonequilibrium.- Sedney et al. (ref. 1) and South (ref. 5) have solved the vibrational nonequilibrium flow field over a wedge by the methods of characteristics and integral relations, respectively. The following case (designated case I) was chosen to compare with the method of characteristics:

Case I: The gas is N_2 and

$$T_\infty = 300^0 \text{ K}$$

$$M_\infty = 6$$

$$\frac{\Theta_V}{T_\infty} = 11.12$$

$$\theta = 40.02^0$$

$$\left(E_V\right)_\infty = 0$$

All lengths were nondimensionalized by

$$L = V_\infty \tau_{x=0}$$

Therefore, the proportionality constant in the relation for τ does not affect the nondimensional variables.

In order to determine the effect of the mesh spacing, two separate computations were performed with initial data lines at $\bar{x}_0 = 0.035$ and at $\bar{x}_0 = 0.1$. Although $\Delta\bar{x}$ and $\Delta\bar{y}$ were smaller for the case with $\bar{x}_0 = 0.035$ than those for $\bar{x}_0 = 0.1$, the ratio $\Delta\bar{x}/\Delta\bar{y}$ was the same for both cases. The flow field was computed downstream to $\bar{x} = 4$ in each case. Figures 7, 8, 9, and 10 show the variation of $\bar{p}$, $\overline{T}$, $\overline{E}_V$, and $\bar{u}$, respectively, along the wedge surface. Agreement with the method of characteristics is very good, except near the starting point. Here the pressure and velocity, in particular, deviate from

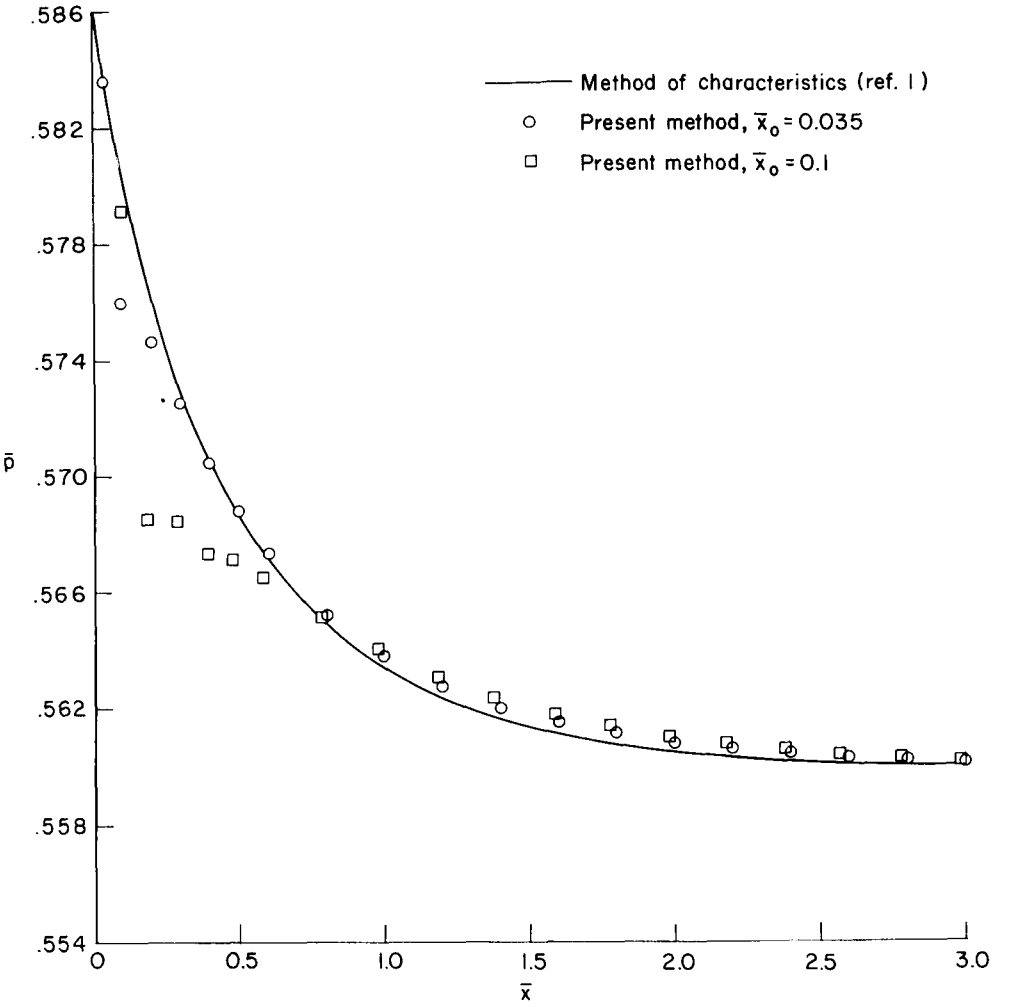

Figure 7.- Pressure along wedge surface for case I.

the correct solution; however, these quantities quickly recover as the calculations are made downstream. The amount of deviation increases with increasing mesh size. On the other hand, figures 8 and 9 show very little deviation in the values of $\overline{T}$ and $\overline{E}_v$ from the characteristics solution.

Figures 11 and 12(a) give the $\bar{p}$ and $\overline{T}$ profiles normal to the surface at $\bar{x} = 4$. Of particular interest are the results in the vicinity of the shock wave where the values of $\bar{p}$ and $\overline{T}$, in the shock layer, drop to free-stream values over a few mesh points; thus the shock wave is smeared over these points. Also, these figures show that a more definitive shock is produced by decreasing the mesh spacing (while $\Delta\bar{x}/\Delta\bar{y}$ is held constant). (It is interesting to note that the computational time was 8.8 minutes for $\bar{x}_0 = 0.035$ and only 2.0 minutes for $\bar{x}_0 = 0.1$.)

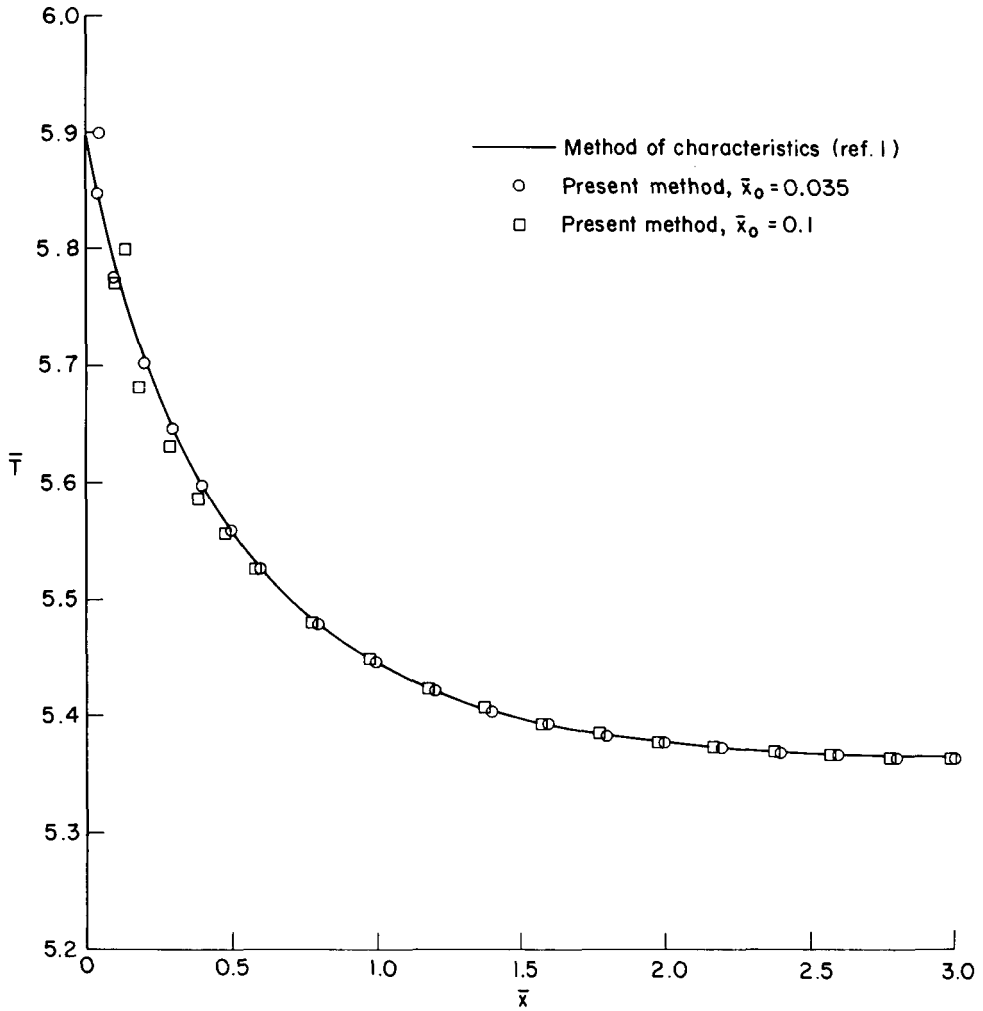

Figure 8.- Temperature along wedge surface for case I.

Figure 12(b) shows a portion of the temperature profile at an expanded scale. This figure illustrates the entropy layer near the surface, a region of near-equilibrium, and the nonequilibrium region near the shock wave proper. Also, there is a significant difference between the actual shock location and that for frozen flow. This difference is due to the fact that the shock wave has the frozen slope at the tip, but bends downward and approaches the slope of an equilibrium flow as $\bar{x}$ increases. (See ref. 1.)

Lighthill's ideal dissociating gas.- Capiaux and Washington (ref. 3) have used the method of characteristics to compute the nonequilibrium flow field over a wedge for Lighthill's ideal dissociating gas. Their technique, however, differs from that used by Sedney in that they used the stream function and distance perpendicular to the wedge axis as independent variables. Newman (ref. 7) also solved this problem by using a modified method of integral relations. The following case (designated case II) was computed by the present method and corresponds to case I in reference 3:

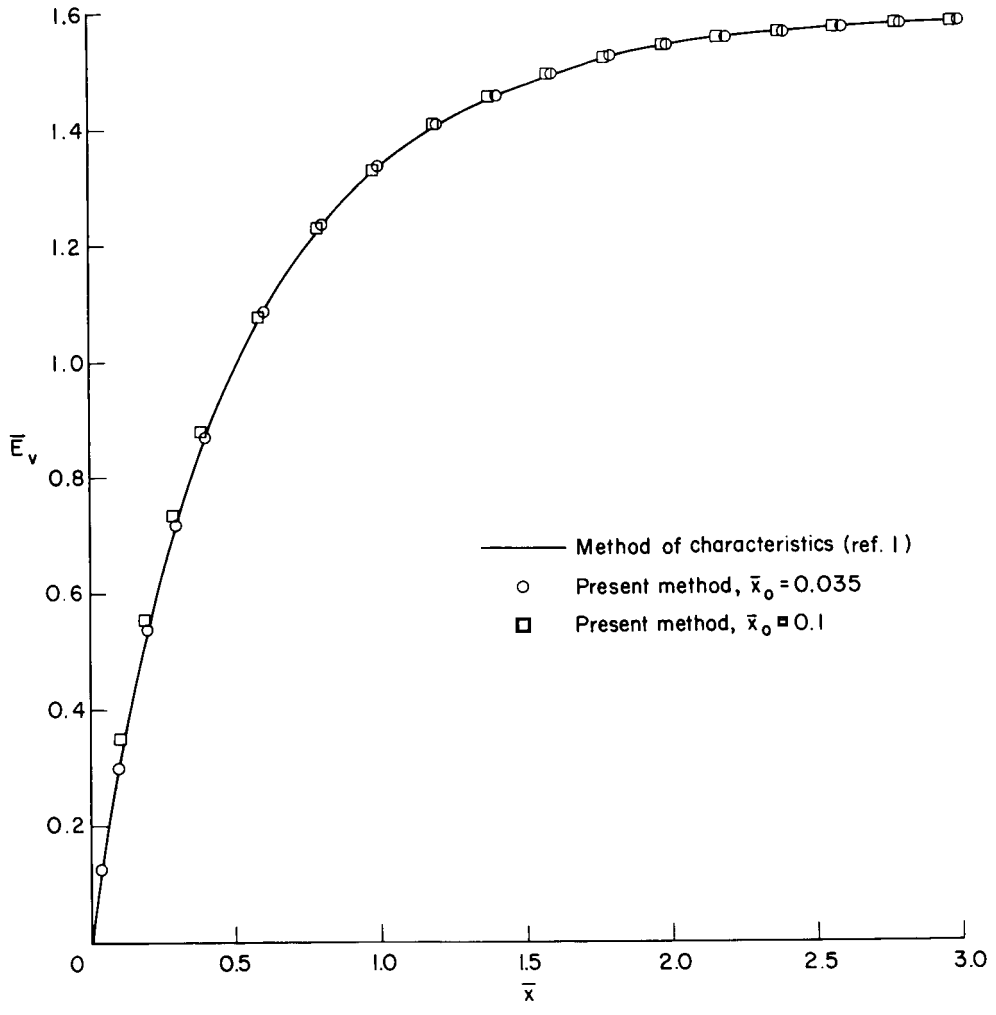

Figure 9.- Vibrational energy along wedge surface for case I.

Case II: The gas is oxygen and

$$\frac{\rho_D}{\rho_\infty} = 0.811 \times 10^8$$

$$M_\infty = 32$$

$$\alpha_\infty = 10^{-10}$$

$$\frac{DN_O}{W_{O_2} V_\infty^2} = 0.15375$$

$$\theta = 25.175^O$$

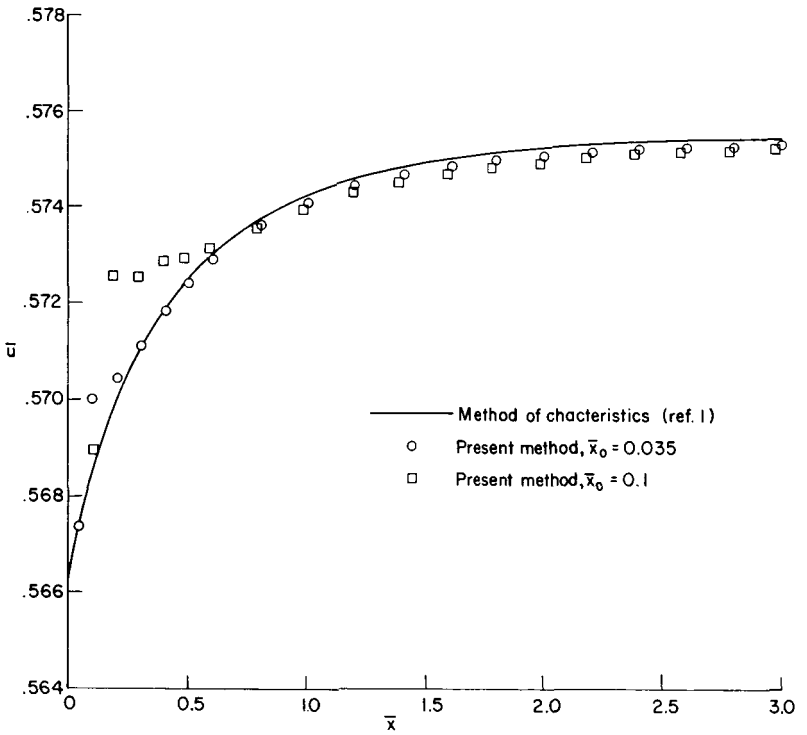

Figure 10.- Velocity along wedge surface for case I.

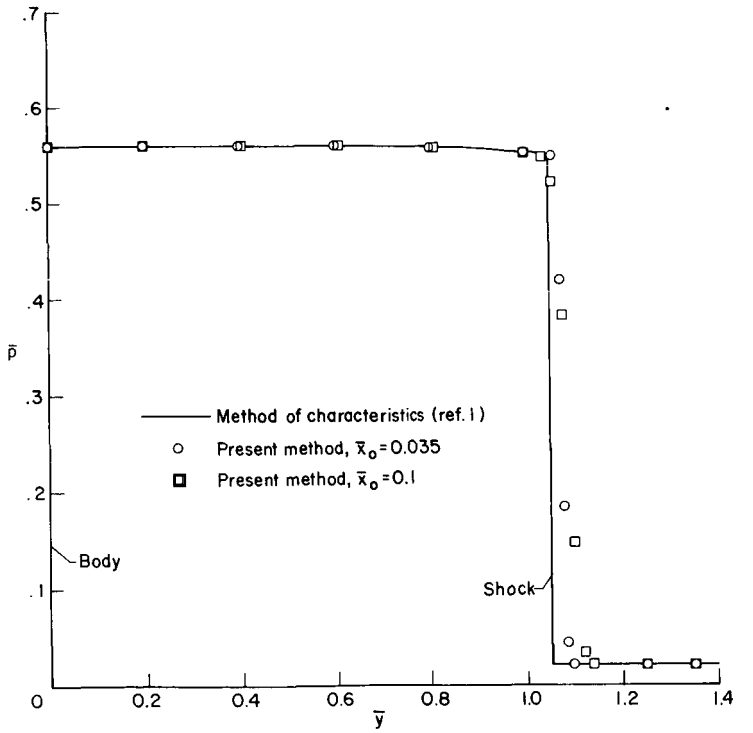

Figure 11.- Pressure profile normal to wedge surface at $\bar{x} = 4$ for case I.

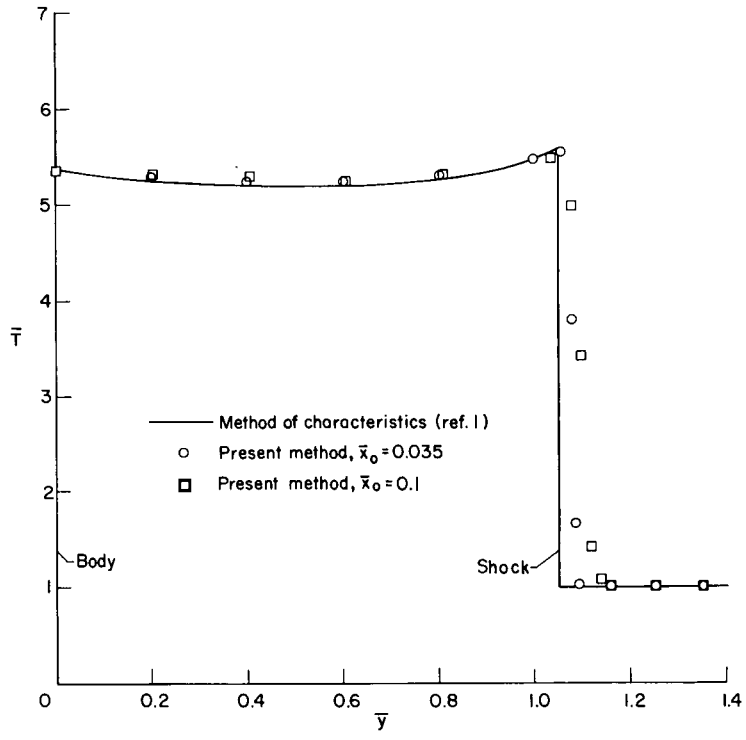

(a) $\bar{x} = 4$; case I.

Figure 12.- Temperature profile normal to wedge surface.

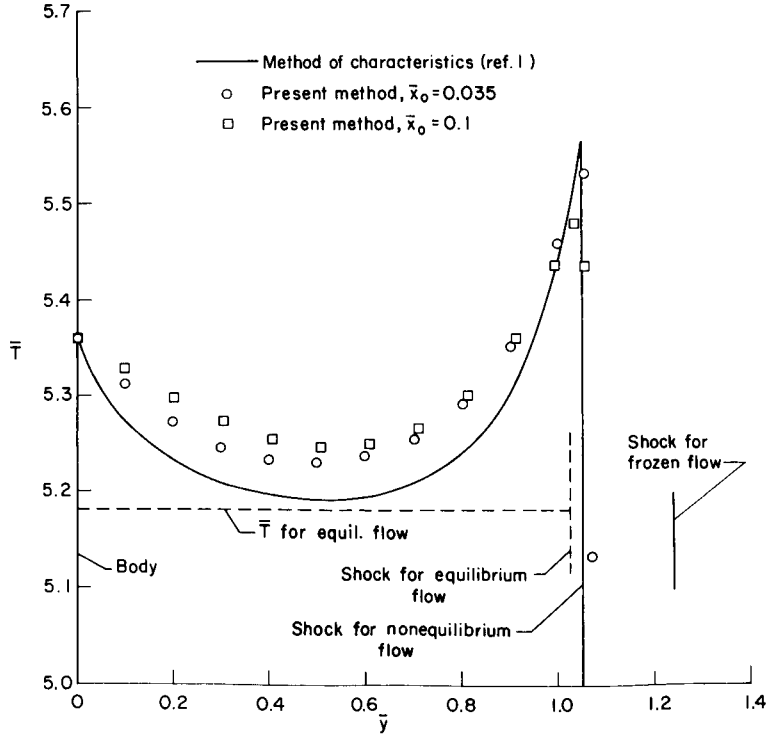

(b) $\bar{x} = 4$; case I; expanded temperature scale.

Figure 12.- Concluded.

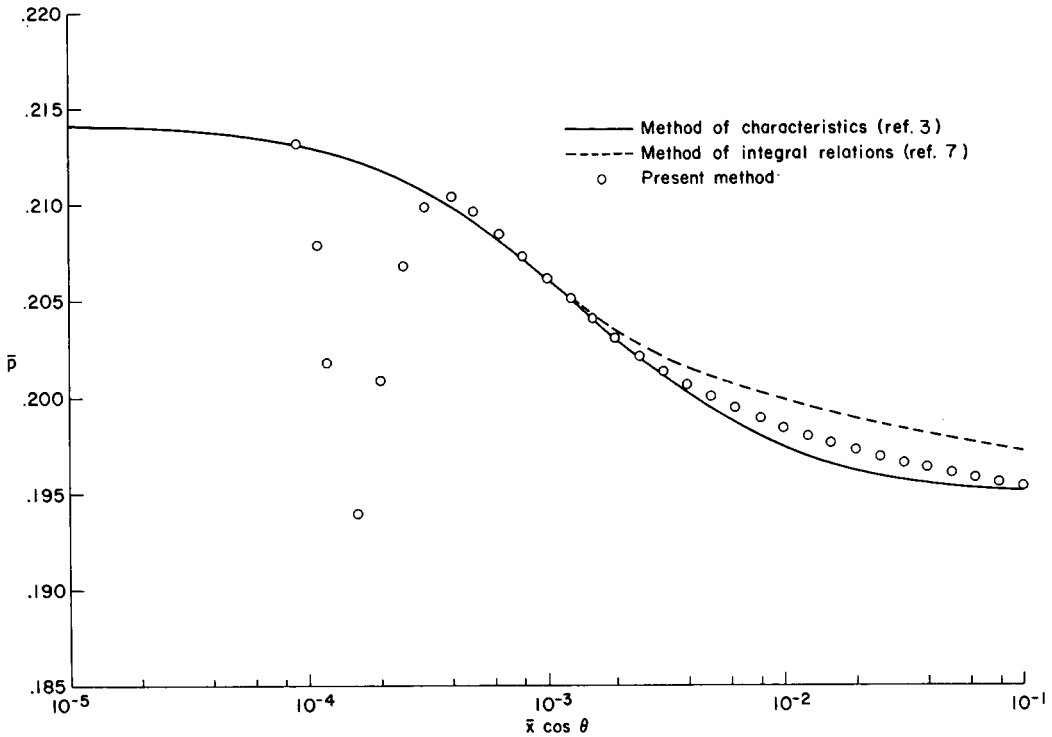

Figure 13.- Variation of surface pressure with axial distance for case II.

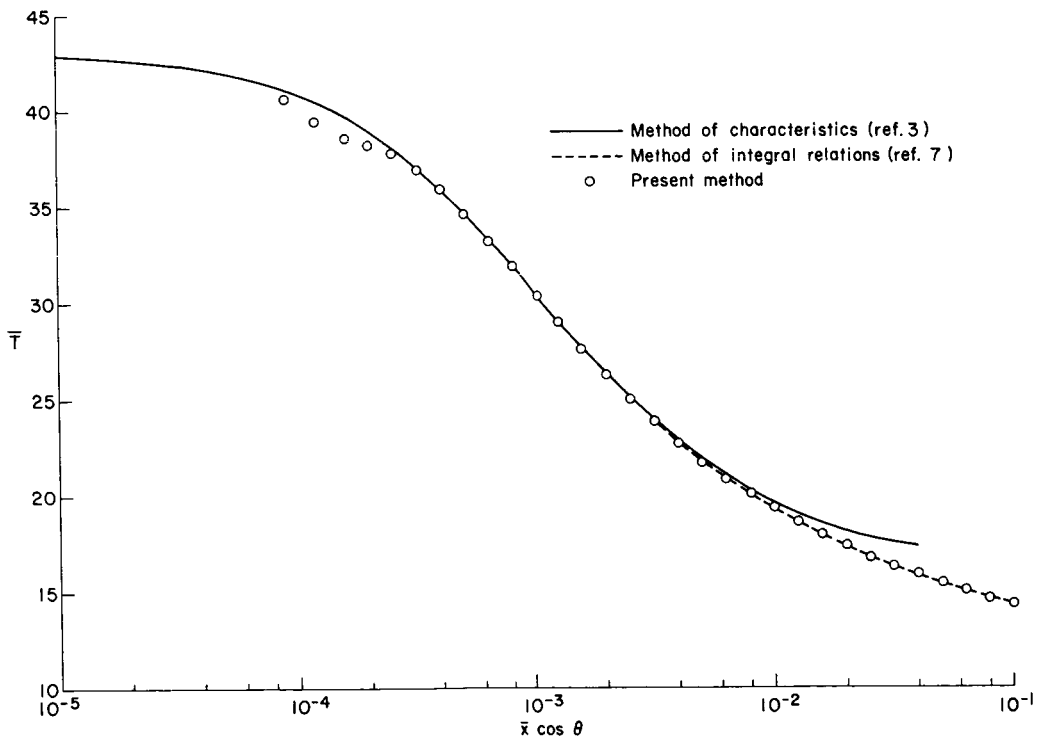

Figure 14.- Variation of surface temperature with axial distance for case II.

All lengths were nondimensionalized by the same length scale as that used in reference 3, that is,

$$L = \frac{V_\infty{}^6}{C^* \rho_\infty} \left(\frac{W_{O_2}}{R} \right)^{2.5}$$

In this manner the numerical value of C^* does not affect the nondimensional properties. Note, however, that reference 7 used a different length scale.

In order to obtain good accuracy near the tip of the wedge, the problem was solved in two parts. First, with an initial data line at $\bar{x}_0 = 10^{-4}$, the solution was carried out to $\bar{x} = 4 \times 10^{-3}$. By using the results already computed at $\bar{x} = 1.18 \times 10^{-3}$, a new initial data line (of two points in the shock layer) was used to carry the solution to $\bar{x} = 0.111$. The second solution partly overlapped the first; therefore, the fluctuations which occur near the starting point would not be present in the region $4 \times 10^{-3} \leqq \bar{x} \leqq 0.111$. These results are plotted in figures 13, 14, and 15 and show the variation of $\bar{p}$, $\overline{T}$, and α, respectively, along the surface. It should be noted that reference 3 measures $\bar{x}$ along the axis of symmetry, whereas the present $\bar{x}$ is along the surface. Therefore, $\bar{x} \cos \theta$ in this report corresponds to $\bar{x}$ in reference 3.

Figure 13 shows that the deviation of $\bar{p}$, near the starting point, is more pronounced than in the previous example for vibrational nonequilibrium. However, it should be noted that $\bar{x} \cos \theta$ is plotted on a logarithmic scale; hence, this deviation extends over a very small distance on a linear scale. For $\bar{x} \cos \theta > 2 \times 10^{-3}$, the present method and that of references 3 and 7 all disagree on the surface pressure. It is not presently known why these results differ, or which is the more correct solution.

Figure 14 shows that the present method and that of reference 7 give the same results for $\overline{T}$ along the surface. The method of reference 3, however, differs from these two methods for $\bar{x} \cos \theta > 3 \times 10^{-3}$. All three methods give essentially the same results for α, as shown in figure 15. (The total computational time for the present method was 16.2 minutes.)

DISCUSSION

The comparisons given in figures 5 to 15 show that the present method correctly calculates the flow field over bodies except near the initial data line. At that point, unrealistic deviations appear in the flow properties on the body but are quickly damped out. It was found that these deviations still occurred even when as many as 20 points were used on the initial data line between the body and the shock wave. The only difference was that the deviations started at a position downstream where the first mesh point outside the shock wave on the initial data line influences a body point. It is believed that these

deviations are caused by using free-stream properties at one mesh point, and shock properties at the mesh point adjacent to it on the initial data line. This procedure causes a weak disturbance to propagate down to the body, and the boundary conditions cause the surface properties to deviate from the correct solution. When other types of coordinate systems and schemes for computing the body points were investigated, the deviations near the initial data line were greater than those of the present method. Also, it was mentioned previously that the y-momentum equation was not used at the surface because it is not needed. (The boundary condition specifies that $v = 0$ on the surface.) Upon investigating the computed flow fields, it was found that the y-momentum equation was not satisfied at the surface in the regions where these deviations occurred. However, downstream where the deviations were damped out, it was found that the y-momentum equation was satisfied at the surface. The present method could be altered to satisfy simultaneously all the equations and boundary conditions on the surface if $\Delta\bar{x}$ was made a variable for each step in the computational procedure. However, this procedure increases the complexity of the method manyfold and may require computational times comparable with the method of characteristics.

Several investigations were performed to determine the effect of using different values of the ratio $\Delta\bar{x}/\Delta\bar{y}$. When this ratio was greater than that given by the stability criterion, the computed flow properties became unstable after only a few mesh spaces downstream of the initial data line. However, for values of $\Delta x/\Delta y$ consistent with the stability criterion, more accurate results were always obtained the closer the mesh system followed the characteristics. This result is illustrated in appendix A.

The staggered mesh system that is used for the finite-difference scheme has the decided advantage that it requires only half as many mesh points as an unstaggered system and yet it gives the same accuracy. This system reduces both the computing machine storage spaces and the computational time by a factor of 2. The present method also has the advantage of using a mesh system that is fixed, whereas the method of characteristics must compute its mesh points. Therefore, the present method requires less computational time than the method of characteristics.

The results obtained show that the present method gives good accuracy even for a large mesh scale. For the flow past a wedge, only two points were used inside the shock layer for the initial data line. The downstream profiles of the flow properties across the shock layer show that the present method gives better accuracy than the method of integral relations. If greater accuracy is desired in the present method, an extrapolation procedure such as described by Roberts (ref. 10) can be used.

In addition to the frozen flow past axially symmetric bodies, the present method has also been applied to nonequilibrium flows over cones. However, since there are no exact expressions for the cone tip gradients like those for wedges, the initial data line was

composed of the frozen cone solution. As a result, the solutions were not very accurate for the mesh spacings used to date. Reference 2 also encountered considerable difficulty in the computation of nonequilibrium flows over cones by the method of characteristics. In reference 2 it was found that a much smaller mesh spacing was needed for cones than for wedges. It is believed that accurate, nonequilibrium cone solutions can be obtained with the present method if a very small mesh spacing was used, or if the cone tip gradients were known.

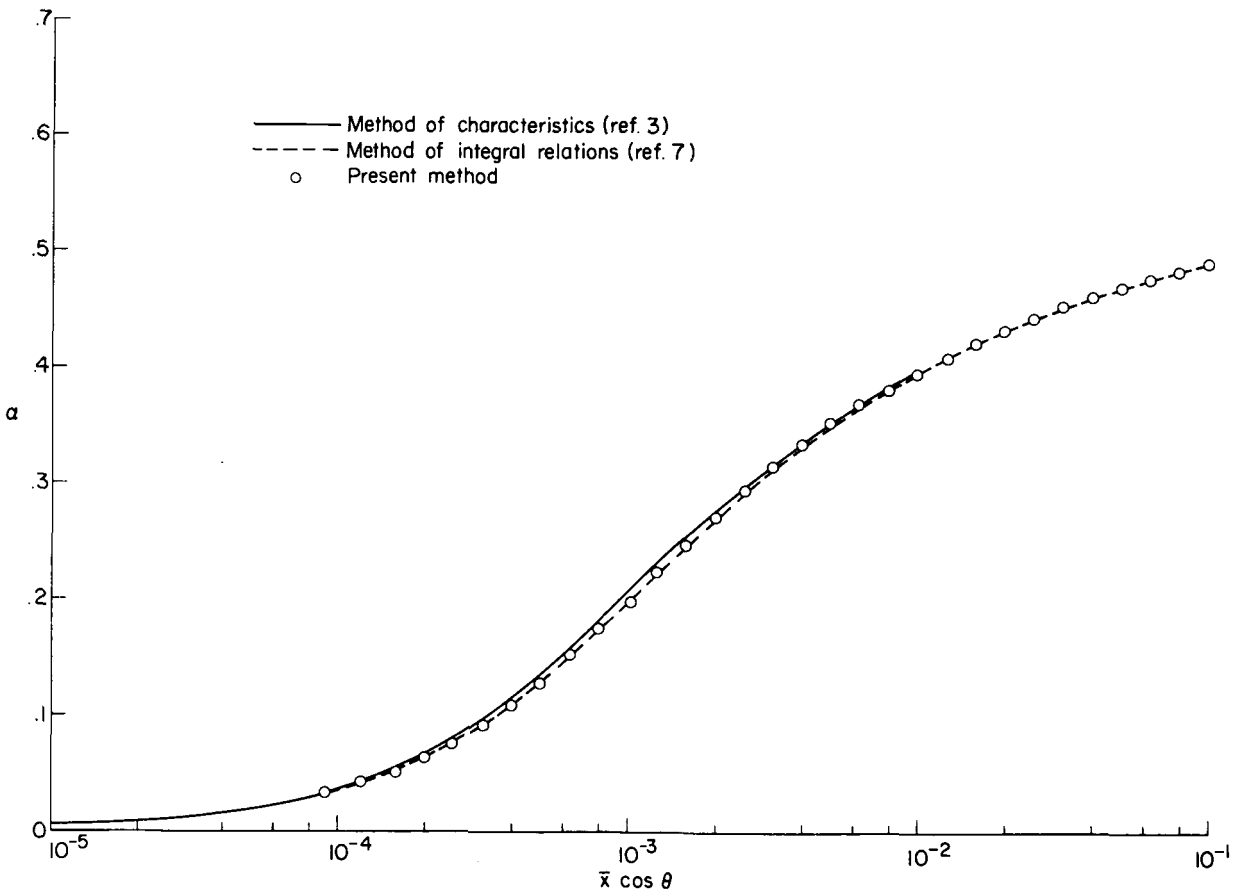

Figure 15.- Variation of surface atom mass fraction with axial distance for case II.

CONCLUSIONS

The finite-difference method developed by P. D. Lax for unsteady flows is applied to the steady-state equations for the supersonic region of inviscid flows past two-dimensional and axisymmetric bodies. A diatomic gas subject to nonequilibrium vibrations and dissociation is considered. As a consequence of Lax's finite-difference scheme, an artificial viscosity is implicitly introduced. This scheme allows the computations to proceed downstream of an initial data line as if no shock wave were present at all. The

shock wave appears in the solution, however, smeared over several mesh spaces while it accurately gives the proper jump conditions across the shock. As a result of the application of this method, the following conclusions can be drawn:

1. The finite-difference method developed herein is applicable to the solution of the supersonic-hypersonic flow fields past two-dimensional and axisymmetric bodies.

2. The numerical results show that the present method compares favorably with the results obtained by the methods of characteristics and integral relations for both perfect- and real-gas flow fields.

3. The new difference scheme developed for the body points is more accurate than extrapolation schemes and reflection principles previously used. The success of this difference scheme is dependent on a body-oriented coordinate system.

4. The staggered mesh system has the advantage of reducing the computations required for an unstaggered mesh system without sacrificing accuracy in the results.

5. The closer the mesh system approaches the characteristics network, the more accurate the results.

6. The present method is sufficiently accurate to yield better profiles of properties across the shock layer than the method of integral relations, yet it is simple enough to require less time for machine computations than the method of characteristics.

Langley Research Center,
National Aeronautics and Space Administration,
Langley Station, Hampton, Va., September 21, 1965.

APPENDIX A

FROZEN FLOW THROUGH AN OBLIQUE SHOCK WAVE

This example illustrates the application of the present method for the computation of a steady flow field without a boundary and is similar to the computations by Lax (ref. 9) for unsteady flow. This case is for an oblique shock wave $(\Omega_F = 30^o)$ positioned in a free stream of $M_\infty = 3$ and $\gamma = 1.4$. The x-axis is parallel to V_∞, and the y-axis is perpendicular to V_∞. Since there is no boundary, the initial data line (n = 0) consists of the free-stream properties at $k = 1, 3, 5, 7, \ldots$ and the frozen shock properties at $k = -1, -3, -5, -7, \ldots$ and places the shock wave at $k = 0$ on the initial data line. The

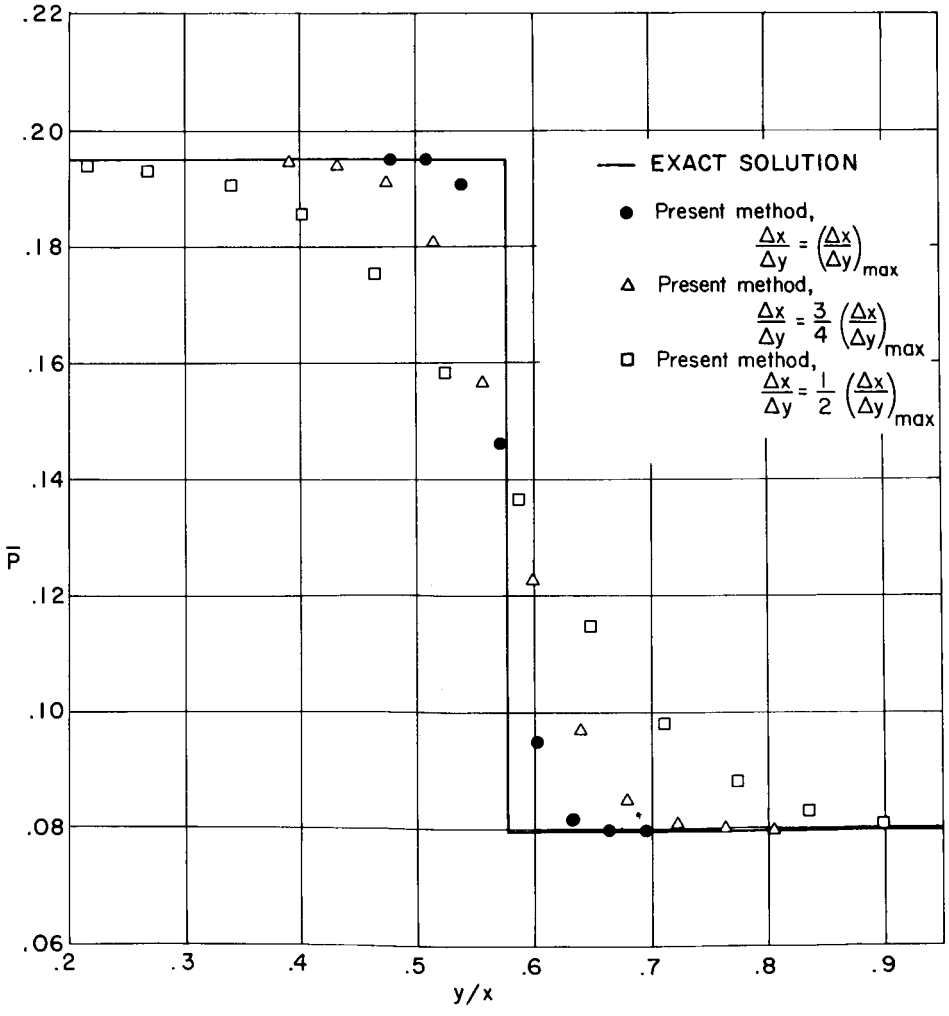

Figure 16.- Pressure profile through an oblique shock wave at $n = 49$ for frozen flow. $M_\infty = 3$; $\Omega_F = 30^o$; $\gamma = 1.4$.

present method has been used to compute the downstream flow field for three values of $\Delta x/\Delta y$. From the stability criterion,

$$\left(\frac{\Delta x}{\Delta y}\right)_{max} = \cot\left[\left|\tan^{-1}\left(\frac{v}{u}\right)_F\right| + \mu\right]_{min} = 1.2910$$

Figure 16 shows the pressure profiles computed at $n = 49$. This figure illustrates that the profile through the shock wave is qualitatively similar to those obtained experimentally in reference 19. It is also seen that the computed shock wave is narrowest when $\frac{\Delta x}{\Delta y} = \left(\frac{\Delta x}{\Delta y}\right)_{max}$, a conclusion noted by Lax in reference 9. The reason for this phenomenon is that the "artificial" coefficient of viscosity $\left(\frac{\Delta \bar{y}^2}{2\,\Delta \bar{x}}\right.$ in eq. (19)$\left.\right)$ decreases as $\Delta \bar{x}/\Delta \bar{y}$ increases ($\Delta \bar{y}$ being held constant).

APPENDIX B

BODY POINTS FOR NONEQUILIBRIUM FLOW

The numerical scheme formulated for the body points computed $a_m + \Delta\bar{x}d_m$ for $m = 1, 2, 4$, and 5 at the new mesh point $n+1,0$ from the known properties at $n,1$ and $n-1,0$. For nonequilibrium flow α and $\overline{E}_v$ are not known at $n+1,0$ and, hence, an iterative technique must be employed to determine the individual fluid properties from $(a_m + \Delta\bar{x}d_m)_{n+1,0}$. The steps in this method are:

(1) Assume

$$(d_4)_{n+1,0} = (d_4)_{n-1,0}\left(\frac{r_{n+1,0}}{r_{n-1,0}}\right)^j$$

and

$$(d_5)_{n+1,0} = (d_5)_{n-1,0}\left(\frac{r_{n+1,0}}{r_{n-1,0}}\right)^j$$

(2) Compute $(\overline{E}_v)_{n+1,0}$ and $\alpha_{n+1,0}$ from

$$(\overline{E}_v)_{n+1,0} = \frac{(a_4 + \Delta\bar{x}d_4)_{n+1,0}}{(a_1)_{n+1,0}} - \frac{(d_4)_{n+1,0}\,\Delta\bar{x}}{(a_1)_{n+1,0}}$$

and

$$\alpha_{n+1,0} = \frac{(a_5 + \Delta\bar{x}d_5)_{n+1,0}}{(a_1)_{n+1,0}} - \frac{(d_5)_{n+1,0}\,\Delta\bar{x}}{(a_1)_{n+1,0}}$$

(3) Compute $\bar{u}_{n+1,0}$ from equation (42), $\bar{\rho}_{n+1,0}$ from equation (43), $\bar{p}_{n+1,0}$ from equation (44), and $\overline{T}_{n+1,0}$ from equation (45).

(4) By using the properties computed in steps (2) and (3), compute new values of $(d_4)_{n+1,0}$ and $(d_5)_{n+1,0}$ from equation (16).

(5) By using the new values of $(d_4)_{n+1,0}$ and $(d_5)_{n+1,0}$, repeat steps (2) to (4) until the temperature found in step (3) differs from its previous value by less than 10^{-3} percent. Convergence usually requires less than five iterations.

APPENDIX C

WEDGE-TIP GRADIENTS

Exact expressions for the wedge-tip gradients have been derived by Sedney et al. (ref. 1) and South (ref. 5) for vibrational nonequilibrium, and by Capiaux and Washington (ref. 3) for Lighthill's ideal dissociating gas. South's derivation gives the results in a form suitable for obtaining the initial data line in the present method. Therefore, the results given in this appendix were obtained in the same manner as outlined in appendixes A and C of reference 5 but were extended to include dissociation.

For frozen shock-wave relations,

$$\gamma_\infty = \frac{7 + 3\alpha_\infty}{5 + \alpha_\infty} \tag{C1}$$

Define F and G as

$$F = M_\infty{}^2 \sin^2 \Omega_F \tag{C2}$$

$$G = \frac{2(F - 1)}{(\gamma_\infty + 1)M_\infty{}^2} \tag{C3}$$

then

$$\cot \theta = \tan \Omega_F \left(\frac{1}{G} - 1\right) \tag{C4}$$

$$\bar{u}_F = (1 - G)\cos \theta + G \cot \Omega_F \sin \theta \tag{C5}$$

$$\bar{v}_F = -(1 - G)\sin \theta + G \cot \Omega_F \cos \theta \tag{C6}$$

$$\bar{p}_F = \frac{2\gamma_\infty F - (\gamma_\infty - 1)}{(\gamma_\infty + 1)\gamma_\infty M_\infty{}^2} \tag{C7}$$

$$\bar{\rho}_F = \frac{(\gamma_\infty + 1)F}{(\gamma_\infty - 1)F + 2} \tag{C8}$$

and

$$\bar{T}_F = \frac{\left[2\gamma_\infty F - (\gamma_\infty - 1)\right]\left[(\gamma_\infty - 1)F + 2\right]}{(\gamma_\infty + 1)^2 F} \tag{C9}$$

APPENDIX C

When derivatives of equations (C5), (C6), and (C7) are taken with respect to Ω_F,

$$\left(\frac{d\bar{u}}{d\Omega}\right)_F = \frac{-4 \cos \Omega_F \sin\left(\Omega_F - \theta\right)}{\left(\gamma_\infty + 1\right)} - \frac{G \sin \theta}{\sin^2 \Omega_F} \tag{C10}$$

$$\left(\frac{d\bar{v}}{d\Omega}\right)_F = \frac{4 \cos \Omega_F \cos\left(\Omega_F - \theta\right)}{\left(\gamma_\infty + 1\right)} - \frac{G \cos \theta}{\sin^2 \Omega_F} \tag{C11}$$

$$\left(\frac{d\bar{p}}{d\Omega}\right)_F = \frac{4 \sin \Omega_F \cos \Omega_F}{\left(\gamma_\infty + 1\right)} \tag{C12}$$

With δ defined as the y-position of the shock wave and $\bar{\delta} = \frac{\delta}{L}$, the wedge-tip gradients are

$$\frac{d\Omega}{d\bar{x}} = \frac{\dfrac{-2\left(1 - \alpha_\infty\right)\dfrac{\Lambda L W A_2}{V_\infty R T_\infty} - \dfrac{\Gamma L}{V_\infty}\left[2\left(1 + \alpha_\infty\right)\left(\bar{\Theta}_D - \bar{E}_{v_\infty}\right) - 4\bar{T}_F\right]}{\bar{T}_F\left(7 + 3\alpha_\infty\right)} \qquad \bar{T}_F\left(7 + 3\alpha_\infty\right)\left(1 + \alpha_\infty\right)}{\dfrac{\left(M_F{}^2 - 1\right)}{\bar{\rho}_F \bar{u}_F}\left(\dfrac{d\bar{p}}{d\Omega}\right)_F + \cot\left(\Omega_F - \theta\right)\left(\dfrac{d\bar{v}}{d\Omega}\right)_F} \tag{C13}$$

$$\frac{d\bar{u}_k}{d\bar{x}} = \left[\frac{y_k}{\delta}\left(\frac{d\bar{u}}{d\Omega}\right)_F - \frac{\left(1 - \dfrac{y_k}{\delta}\right)}{\bar{\rho}_F \bar{u}_F}\left(\frac{d\bar{p}}{d\Omega}\right)_F\right]\left(\frac{d\Omega}{d\bar{x}}\right) \tag{C14}$$

$$\frac{d\bar{v}_k}{d\bar{x}} = \frac{y_k}{\delta}\left(\frac{d\bar{v}}{d\Omega}\right)_F\left(\frac{d\Omega}{d\bar{x}}\right) \tag{C15}$$

$$\frac{d\bar{p}_k}{d\bar{x}} = \left(\frac{d\bar{p}}{d\Omega}\right)_F\left(\frac{d\Omega}{d\bar{x}}\right) \tag{C16}$$

$$\frac{d\left(\bar{E}_v\right)_k}{d\bar{x}} = \left(1 - \frac{y_k}{\delta}\right)\frac{\Lambda}{\bar{u}_F}\frac{L W A_2}{R T_\infty V_\infty} \tag{C17}$$

$$\frac{d\alpha_k}{d\bar{x}} = \left(1 - \frac{y_k}{\delta}\right)\frac{\Gamma}{\bar{u}_F}\frac{L}{V_\infty} \tag{C18}$$

By using these tip gradients and neglecting second and higher order terms, the flow properties across the shock layer at the distance $\bar{x}_o$ (n = 0) from the tip may be written as

$$\bar{u}_{o,k} = \bar{u}_F + \left(\frac{d\bar{u}_k}{d\bar{x}}\right)\bar{x}_o \tag{C19}$$

$$\bar{v}_{o,k} = \left(\frac{d\bar{v}_k}{d\bar{x}}\right)\bar{x}_o \tag{C20}$$

$$\bar{p}_{o,k} = \bar{p}_F + \left(\frac{d\bar{p}_k}{d\bar{x}}\right)\bar{x}_o \tag{C21}$$

$$\left(\overline{E}_v\right)_{o,k} = \overline{E}_{v_\infty} + \left[\frac{d\left(\overline{E}_v\right)_k}{d\bar{x}}\right]\bar{x}_o \tag{C22}$$

and

$$\alpha_{o,k} = \alpha_\infty + \left(\frac{d\alpha_k}{d\bar{x}}\right)\bar{x}_o \tag{C23}$$

By using these properties, $\overline{T}_{o,k}$ may be obtained from the energy equation and then $\bar{\rho}_{o,k}$ from the equation of state. Since $\frac{d\bar{\delta}}{d\bar{x}} = \tan(\Omega - \theta)$, the shock position $\bar{\delta}$ at $\bar{x}_o$ is (third and higher order terms being neglected)

$$\bar{\delta} = \tan\left(\Omega_F - \theta\right)\bar{x}_o + \sec^2\left(\Omega_F - \theta\right)\left(\frac{d\Omega}{d\bar{x}}\right)\frac{\bar{x}_o^2}{2} \tag{C24}$$

When Lighthill's gas is considered, the only changes required are that equations (C1) and (C13) be replaced by

$$\gamma_\infty = \frac{4 + \alpha_\infty}{3} \tag{C25}$$

$$\frac{d\Omega}{d\bar{x}} = \frac{-\frac{\Gamma L}{V_\infty}\left[\left(1 + \alpha_\infty\right)\bar{\Theta}_D - 3\overline{T}_F\right]}{\overline{T}_F\left(1 + \alpha_\infty\right)\left(4 + \alpha_\infty\right)} \Bigg/ \left[\frac{\left(M_F^2 - 1\right)}{\bar{\rho}_F\bar{u}_F}\left(\frac{d\bar{p}}{d\Omega}\right)_F + \cot\left(\Omega_F - \theta\right)\left(\frac{d\bar{v}}{d\Omega}\right)_F\right] \tag{C26}$$

and equations (C17) and (C22) are not needed.

REFERENCES

1. Sedney, R.; South, J. C.; and Gerber, N.: Characteristic Calculation of Non-Equilibrium Flows. Rept. No. 1173, Ballistic Research Labs., Aberdeen Proving Ground, Apr. 1962.

2. Sedney, R.; and Gerber, N.: Nonequilibrium Flow Over a Cone. AIAA J., vol. 1, no. 11, Nov. 1963, pp. 2482-2486.

3. Capiaux, R.; and Washington, M.: Nonequilibrium Flow Past a Wedge. AIAA J., vol. 1, no. 3, Mar. 1963, pp. 650-660.

4. Marrone, Paul V.: Inviscid, Nonequilibrium Flow Behind Bow and Normal Shock Waves, Part I. General Analysis and Numerical Examples. Rept. No. QM-1626-A-12(I) (Contract No. DA-30-069-0RD-3443), Cornell Aeron. Lab., Inc., May 1963.

5. South, Jerry C., Jr.: Application of the Method of Integral Relations to Supersonic Nonequilibrium Flow Past Wedges and Cones. NASA TR R-205, 1964.

6. Shih, William C. L.; Baron, Judson R.; Krupp, Roy S.; and Towle, William J.: Nonequilibrium Blunt Body Flow Using the Method of Integral Relations. Tech. Rept. 66 (Contract NOw 62-0765-d), Aerophys. Lab., M.I.T., May 1963. (Available from DDC as 415934.)

7. Newman, Perry A.: A Modified Method of Integral Relations for Supersonic Non-equilibrium Flow Over a Wedge. NASA TN D-2654, 1965.

8. Lin, S. C.; and Teare, J. D.: A Streamtube Approximation for Calculation of Reaction Rates in the Inviscid Flow Field of Hypersonic Objects. Re-entry. Vol. IV of Ballistic Missile and Aerospace Technology, C. T. Morrow, L. D. Ely, and M. R. Smith, eds., Academic Press, c.1961, pp. 35-50.

9. Lax, Peter D.: Weak Solutions of Nonlinear Hyperbolic Equations and Their Numerical Computation. Commun. Pure Appl. Math., vol. VII, no. 1, Feb. 1954, pp. 159-193.

10. Roberts, Leonard: On the Numerical Solution of the Equations for Spherical Waves of Finite Amplitude, II. J. Math. Phys., vol. XXXVI, no. 4, Jan. 1958, pp. 329-337.

11. Bohachevsky, Ihor O.; Rubin, Ephraim L.; and Mates, Robert E.: A Direct Method for Computation of Nonequilibrium Flows With Detached Shock Waves. Paper No. 65-24, Am. Inst. Aeron. Astronaut., Jan. 1965.

12. Lax, Peter D.; and Wendroff, Burton: Difference Schemes for Hyperbolic Equations With High Order of Accuracy. Commun. Pure Appl. Math., vol. XVII, no. 3, Aug. 1964, pp. 381-398.

13. Burstein, Samuel Z.: Numerical Methods in Multidimensional Shocked Flows. AIAA J., vol. 2, no. 12, Dec. 1964, pp. 2111-2117.

14. Thommen, Hans U; and D'Attorre, Leonardo: Calculation of Steady, Three-Dimensional Supersonic Flow-Fields by a Finite Difference Method. Paper No. 65-26, Am. Inst. Aeron. Astronaut., Jan. 1965.

15. VonNeumann, J.; and Richtmyer, R. D.: A Method for Numerical Calculation of Hydrodynamic Shocks. J. Appl. Phys., vol. 21, no. 3, Mar. 1950, pp. 232-237.

16. DeJarnette, Fred R.: Numerical Solution of Inviscid Hypersonic Flows for Non-equilibrium Vibration and Dissociation Using an "Artificial Viscosity" Method. Ph.D. Thesis, Virginia Polytech. Inst., Mar. 1965.

17. Lighthill, M. J.: Dynamics of a Dissociating Gas. Part I – Equilibrium Flow. J. Fluid Mech., vol. 2, pt. 1, Jan. 1957, pp. 1-32.

18. Fluid Motion Sub-Committee of the Aeronautical Research Council: Modern Developments in Fluid Dynamics. High Speed Flow. Vols. I and II, L. Howarth, ed., The Clarendon Press (Oxford), 1953.

19. Sherman, F. S.: A Low-Density Wind-Tunnel Study of Shock-Wave Structure and Relaxation Phenomena in Gases. NACA TN 3298, 1955.

20. Courant, R.; Friedrichs, K.; and Lewy, H.: Über die partiellen Differenzengleichungen der mathematishen Physik. Math. Ann., vol. 100, 1928, pp. 32-74.

21. Wood, William W.; and Kirkwood, John G.: Hydrodynamics of a Reacting and Relaxing Fluid. J. Appl. Phys., vol. 28, no. 4, Apr. 1957, pp. 395-398.

22. Shapiro, Ascher H.: The Dynamics and Thermodynamics of Compressible Fluid Flow. Vol. I. The Ronald Press Co., c.1953.

23. Sedney, Raymond: Some Aspects of Nonequilibrium Flows. J. Aerospace Sci., vol. 28, no. 3, Mar. 1961, pp. 189-196, 208.

24. Taylor, G. I.; and Maccoll, J. W.: The Air Pressure on a Cone Moving at High Speeds. Proc. Roy. Soc. (London), ser. A, vol. 139, no. 838, Feb. 1, 1933, pp. 278-311.

"The aeronautical and space activities of the United States shall be conducted so as to contribute . . . to the expansion of human knowledge of phenomena in the atmosphere and space. The Administration shall provide for the widest practicable and appropriate dissemination of information concerning its activities and the results thereof."

—NATIONAL AERONAUTICS AND SPACE ACT OF 1958

NASA SCIENTIFIC AND TECHNICAL PUBLICATIONS

TECHNICAL REPORTS: Scientific and technical information considered important, complete, and a lasting contribution to existing knowledge.

TECHNICAL NOTES: Information less broad in scope but nevertheless of importance as a contribution to existing knowledge.

TECHNICAL MEMORANDUMS: Information receiving limited distribution because of preliminary data, security classification, or other reasons.

CONTRACTOR REPORTS: Technical information generated in connection with a NASA contract or grant and released under NASA auspices.

TECHNICAL TRANSLATIONS: Information published in a foreign language considered to merit NASA distribution in English.

TECHNICAL REPRINTS: Information derived from NASA activities and initially published in the form of journal articles.

SPECIAL PUBLICATIONS: Information derived from or of value to NASA activities but not necessarily reporting the results of individual NASA-programmed scientific efforts. Publications include conference proceedings, monographs, data compilations, handbooks, sourcebooks, and special bibliographies.

Details on the availability of these publications may be obtained from:

SCIENTIFIC AND TECHNICAL INFORMATION DIVISION

NATIONAL AERONAUTICS AND SPACE ADMINISTRATION

Washington, D.C. 20546